



HAL
open science

Luminescence Properties of CdTe and CdZnTe Materials When Used as Substrate for IR Detectors

Thibault Pichon, Salima Mouzali, Olivier Boulade, Alain Lusson, Giacomo Badano, Jean-Louis Santailler, Névine Rochat, Olivier Gravrand, Olivier Limousin

► **To cite this version:**

Thibault Pichon, Salima Mouzali, Olivier Boulade, Alain Lusson, Giacomo Badano, et al.. Luminescence Properties of CdTe and CdZnTe Materials When Used as Substrate for IR Detectors. *Journal of Electronic Materials*, 2023, 52, pp.3013-3024. 10.1007/s11664-023-10406-w . hal-04075507

HAL Id: hal-04075507

<https://hal.science/hal-04075507>

Submitted on 3 Nov 2023

HAL is a multi-disciplinary open access archive for the deposit and dissemination of scientific research documents, whether they are published or not. The documents may come from teaching and research institutions in France or abroad, or from public or private research centers.

L'archive ouverte pluridisciplinaire **HAL**, est destinée au dépôt et à la diffusion de documents scientifiques de niveau recherche, publiés ou non, émanant des établissements d'enseignement et de recherche français ou étrangers, des laboratoires publics ou privés.

Luminescence properties of CdTe and CdZnTe materials when used as substrate for IR detectors

Thibault Pichon^{a*}, Salima Mouzali^a, Olivier Boulade^a, Alain Lusson^b, Giacomo Badano^c, Jean-Louis Santailier^c,
Névine Rochat^c, Olivier Gravrand^c, Olivier Limousin^a

^aAIM, CEA, CNRS, Université Paris-Saclay, Université Paris Diderot, Sorbonne Paris Cité, F-91191 Gif-sur-Yvette, France

^bUniversité Paris-Saclay, CNRS, Université de Versailles St Quentin en Yvelines, Groupe d'étude de la matière condensée (GEMAC), 45 Avenue des États-Unis, 78035 Versailles, France

^cUniversité Grenoble Alpes, CEA/LETI, 17 Avenue des Martyrs, 38054 Grenoble cedex 9, France

*Corresponding author: thibault.pichon@cea.fr

Abstract

I – Introduction

$\text{Cd}_{1-x}\text{Zn}_x\text{Te}$ is a ternary alloy composed of atoms from columns II and VI of the periodic table. The amount of zinc can be tuned depending on the targeted applications, and the electrical properties vary as the amount of zinc is modified. Its high Z number and its high density make the $\text{Cd}_{1-x}\text{Zn}_x\text{Te}$ semiconductor a suited material for high-performance X-ray and gamma ray detectors for astrophysical and medical applications [1]. Moreover, the CdTe material is widely used in solar cells thanks to its high absorption coefficient in the visible domain [2]. The $\text{Cd}_{1-x}\text{Zn}_x\text{Te}$ is also used as a substrate material in the fabrication process of infrared (IR) detectors based on HgCdTe technology. The amount of zinc in the alloy is tuned to match the lattice parameter of the epitaxial layer of HgCdTe reducing interfacial defects which may degrade the performance of IR detectors. Generally, the amount of zinc in the alloy when used as substrate for HgCdTe-based IR detectors is approximately equal to 4 % [3].

Indeed, the state-of-the-art IR detectors use CdZnTe material as substrate. These IR detectors may then be embarked inside the instruments of satellites. However, space is a harsh environment. In orbit, the satellite and its instruments are impacted by energetic ions (mainly protons) coming from the sun or galactic cosmic rays. Proton irradiation test campaigns on IR detectors have shown an unexpected increase of the detector background under irradiation [4]–[6]. Bright diffuse spots around the protons impact were observed. This pollution of the detector image under irradiation was suspected to be linked to energy deposition inside the $\text{Cd}_{1-x}\text{Zn}_x\text{Te}$ substrate, where the carriers excited by the passage of the proton inside the substrate lose their energy by emitting photons which are in turn detected by the HgCdTe layer. Thus, a parasitic photonic signal adds up to the useful photonic signal and degrades the detector's sensitivity.

It has been shown, that a complete removal of the substrate solves radically the problem [7]–[9], but it constitutes a costly step in the fabrication process. Other published results stated that partially-removed-substrate detectors do not show any increase in the measured background when submitted to proton irradiation [10]. The underlying physical phenomena responsible for the image pollution under irradiation is not fully understood. In our previous work, we adopted a modelling approach in order better understand the latter phenomena and estimate the effect of luminescence in the CdZnTe substrate on the response of IR HgCdTe-based detectors under irradiation [11]. In this model, the optical parameters of CdZnTe material are crucial (particularly the absorption coefficient and energy of the photon emitted by spontaneous emission). In astrophysics, IR detectors are operated at low temperatures (typically 100 K in the short-wave IR domain) to reduce the dark current and increase the sensitivity. Up to our knowledge, not all necessary data are available at these operating temperatures for CdZnTe with low zinc concentrations. Moreover, attention should be paid to low light level luminescence emission as these detectors are very sensitive. Typical dark current measured on these detectors are around 0.01 e-/s/pixel [12].

Hence, we have performed luminescence measurements at different temperatures ranging from 4 K to 300 K, in order to get insight into the recombination processes involved. This gives us the energy of the photons emitted by spontaneous emission inside the substrate under irradiation. This information is of primary importance since photons with lower energy (emitted through defect related recombinations) will be less efficiently absorbed within the substrate. Consequently, they will propagate over long distances and pollute large areas. Moreover, in order to compute optical propagation losses as function of photon energy, absorption coefficient was obtained experimentally with ellipsometry measurements at 80 K, 100 K and 300 K. Specific importance is given to optical

parameters measurements performed at 100 K and 80 K. The first temperature corresponds to the nominal operating temperature of short-wave IR detectors. The second temperature corresponds to the operating temperature of IR detectors, which have been irradiated during an irradiation campaign to validate our model [11][13]. During this experiment, two detectors with two different substrate thicknesses were submitted to 63 MeV proton irradiation. The details of the experiment are given in [13]. The transient events induced by the interaction of the protons with the detector material were experimentally characterized and compared to the simulated ones. The simulations were performed using CdZnTe material properties reported in this paper. In our study, two CdZnTe samples were submitted to luminescence experiment with two different sample quality; an additional objective was to link crystal quality with features observed in luminescence spectra.

The first section describes the samples used in the experiment. Photoluminescence (PL) measurements were performed on these samples from 4 K to 50 K to get insight into the involved recombination processes using representative CdZnTe samples used in the fabrication of IR detectors. The details of the PL experiment and the interpretation of PL spectra are given in section III. As PL signal was unresolvable above 50 K, further cathodoluminescence (CL) measurements were carried out at higher temperatures 300 K, 100 K and 80 K. The results are presented and discussed in section IV, they show that excitonic recombinations dominate CL spectra up to 100 K and probably up to 300 K. In section V, the dielectric function measurements at 80 K, 100 K and 300 K are presented, where the values are extracted from ellipsometry measurements. Eventually, the results of the different experiments are compared to the literature and a formula describing the bandgap energy evolution with temperature is proposed, for CdZnTe material with low zinc concentration.

II – Samples

$Cd_{1-x}Zn_xTe$ is a II-VI ternary semiconductor compound, which is usually grown from the melt (melting point of CdTe is close to 1094°C). At CEA / LETI we develop a Vertical Gradient Freeze Method (VFG) under controlled pressure of cadmium. These methods, allows the growth of $Cd_{1-x}Zn_xTe$ single crystal up to 148 mm in diameter. Growth from closed environment is mandatory if one wants to obtain high quality $Cd_{1-x}Zn_xTe$ crystal. Compound stoichiometry (free of secondary phase defects, which occurred frequently) is difficult to obtain. Second the coefficient of segregation of Zinc into CdTe is greater than 1 ($K_{Zn} \sim 1,33$) meaning that the $Cd_{1-x}Zn_xTe$ crystal presents continuously from the first solidified part, a more Zn rich compound compared to the last solidified part of the crystal which is Zn poor. We obtain the two samples A and B from two different growth runs. We extract sample A at the end of the growth and sample B is prepared at the beginning of the growth. Samples are accurately oriented with main face perpendicular to the $\langle 111 \rangle$ direction and then polished. A chemical etching enables to eliminate the subsurface damages at the end of the preparation stage. CdZnTe sample B shows a lower density of defects seeable with IR transmission microscope than CdZnTe sample A. Hence, the crystal quality of CdZnTe sample B is expected to be better than the one CdZnTe sample A.

CdTe semi-conductor material is more widely studied in the literature than CdZnTe ternary alloy. Consequently, a CdTe sample was submitted to the same measurements and is used as a reference sample to interpret the luminescence spectra. The CdTe sample was fabricated on the same fabrication line with the VGF method.

The characteristic of the samples and the measurements performed are summarized on Table 1.

Table 1 - Summary of the material properties of CdTe and CdZnTe samples and measurements performed.

	CdZnTe A	CdZnTe B	CdTe
<i>Cristal properties</i>			
<i>Orientation</i>	$\langle 111 \rangle$	$\langle 111 \rangle$	$\langle 100 \rangle$
<i>State of the front side</i>	Polished	Polished	Polished
<i>State of the rear side</i>	Frosted	Frosted	Frosted
<i>Chemical treatment (bromine/methanol)</i>	Yes	Yes	Yes
<i>HCl treatment</i>	Yes	Yes	Yes
<i>Expected crystal quality</i>	Bad	Good	Good
<i>Measurements</i>			
<i>Photoluminescence</i>	Yes	Yes	Yes
<i>Cathodoluminescence</i>	Yes	Yes	Yes
<i>Ellipsometry</i>	Yes	No	Yes

III – Photoluminescence measurements

In this section, we present photoluminescence (PL) spectra measurements for CdTe and CdZnTe samples at different temperatures. To analyze these results, each spectrum will be divided into three regions: the band edge emission region (close to the bandgap), the Donor-Acceptor Pair (DAP) region, and the deep emission region. The goal is to understand the different recombination mechanism involved at infrared (IR) detectors operating temperature (100 K and 80 K in our case) from low temperature spectra. And eventually, determine the energy of the photons emitted through radiative recombination in the CdZnTe substrate, which are suspected to be the source of image pollution under proton irradiation in HgCdTe-based IR detectors.

1- Experimental set-up

The samples are installed in a cryostat which allows for photoluminescence study from 4 K to 300 K: they are arranged to a cold finger and a resistance is mounted on the support to control the temperature. The PL signal passes through a glass window before entering the spectrometer. An argon type green laser, emitting at 514 nm was used to excite the carriers in the semiconductor, operating at 10 mW. The laser is focused on the sample with a lens. The harmonic emissions of the laser are suppressed with a filter. Converging mirrors collect the PL light and focus it at the entrance of a Michelson type Fourier Transform Infrared (FTIR) spectrometer. It is composed of two orthogonal mirrors, a beam splitter and a movable mirror allowing to choose between a silicon and a germanium detector.

The detector is a silicon photodiode detector which measures the PL signal from the visible to the Near Infrared Range (NIR), that is to say: $400 \text{ nm} < \lambda < 1100 \text{ nm}$. Filters are used to get rid of the ambient light. PL spectra are extracted by a calculator from the inverse transform of the PL interferogram. The spectra were acquired at different temperatures, from 4 K to 100 K. At higher temperatures, the PL signal was not strong enough to be distinguishable from the noise. In the following subsequent sections, CdTe and CdZnTe spectra are presented and discussed regarding literature data.

2- Photoluminescence results

In order to interpret the CdZnTe luminescence spectra, measurements were firstly done on one CdTe sample. In the literature, the CdTe semiconductor is more widely studied than the CdZnTe material. Hence, as the samples come from the same fabrication lines, the CdTe sample will be used as a reference to analyze the CdZnTe PL spectra. On **Fig. 1**, the PL spectrum of the CdTe sample is plotted with the PL spectra of the CdZnTe samples at 4 K, in log scale. On this plot, the spectra are arbitrary shifted vertically for clarity. The three emissions regions are explicitly shown on **Fig. 1**.

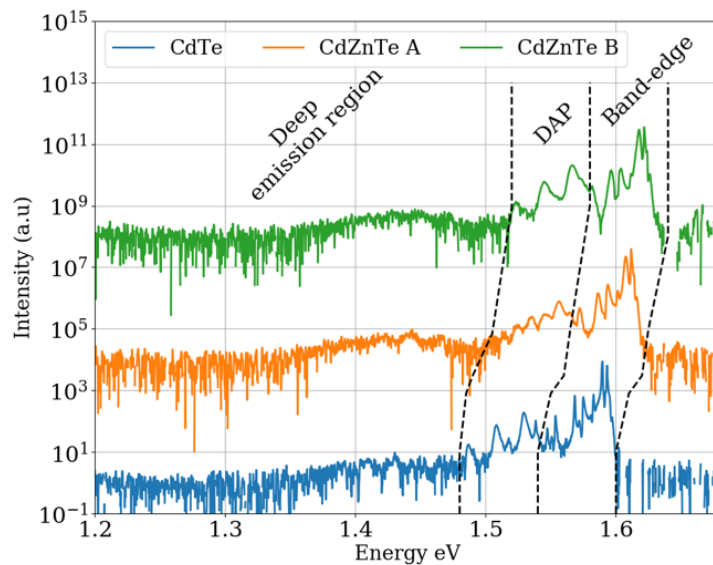


Fig. 1. Photoluminescence spectrum of CdTe and CdZnTe samples at 4 K acquired with a silicon photodiode detector. Log scale

Some common features are visible on these spectra. For instance, it is clear from Fig. 1, that for each sample, light is emitted mostly at the band gap energy. Close to the band-gap, the PL spectra are dominated by excitonic emissions. At lower energies, comes the DAP emission region, which is resolvable at 4 K in each sample. Below the DAP region, a weak (about 1000 times lower than the main emission region) and broad emission band is visible. This emission region is associated with the presence of deep defects in the semi-conductor material.

Nonetheless, some differences are also visible between the spectra of CdTe and CdZnTe. First, the intensities of the CdZnTe PL spectra are slightly lower than the CdTe one. This can be explained by a different surface quality or less efficient radiative transitions in the ternary alloys. Second, the emission lines are broader for CdZnTe which may be due to statistical fluctuations in the atoms concentration in the crystal [14]. Regarding the DAP region, its shape is identical in the CdTe sample and in the CdZnTe sample B, but looks different in CdZnTe sample A.

PL spectra were acquired at different temperature ranging from 4 K to 50 K, above 50 K the PL signal was too weak and could only be hardly distinguishable from the noise. In each sample, the band observed at 4 K in the deep emission region, not shown on Fig. 2, remains weak, and its intensity decreases rapidly as the temperature increases. The PL spectra of the CdTe and CdZnTe are plotted on Fig. 2 for different temperatures considering only the band-edge and DAP emission regions (the spectra are displaced vertically for clarity). It is clear on Fig. 2, that the band-edge emission region dominates the PL spectra of each sample at each temperature. As the temperature increases, the PL intensity decreases. Regarding the DAP emission regions, they are identical in the CdTe and in the CdZnTe B, and their temperature evolution are similar. However, the shape of the DAP emission region of the CdZnTe sample A, is different, which may signify that, different impurities are involved in the recombination process. This emission region will be further studied in this article.

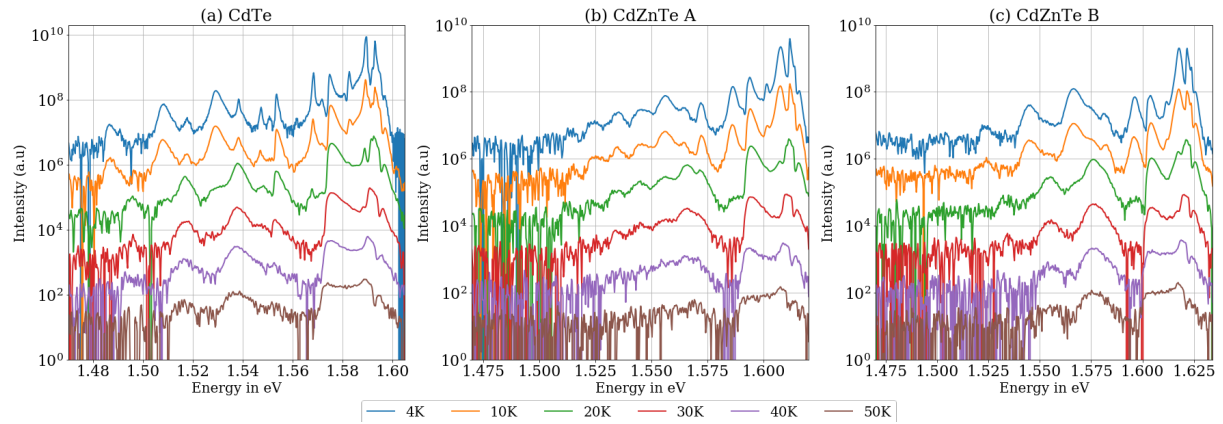


Fig. 2 - Temperature evolution of the PL spectra of the CdTe and CdZnTe samples. The spectra are vertically displaced for clarity

In the following, the interpretations of the PL spectra are done considering successively the 3 emission regions above mentioned and explicitly shown on Fig. 1 : that is to say the band-edge emission region, the DAP emission region and the deep region of emission. We start with the band-edge emission region.

a) Study of PL band-edge emission region from 4 K to 50 K

As already mentioned, in each sample, the band edge emission region is the more intense. It is mainly due to excitonic recombinations (free or bounds) together with their phonon replicas. In this article, emission lines corresponding to the annihilation of free excitons will be denoted (FX). Those related to recombination of an exciton bound to neutral impurities will be noted $A^{\circ}X$, when acceptors impurities come into play, and $D^{\circ}X$ when donors impurities are involved. As CdTe semi-conductor material is more widely studied in the literature, we will first concentrate on this sample. The measured CdTe band edge spectrum at 4 K is given in Fig. 3. This plot is a focus of the band edge emission region of the PL spectrum of the CdTe sample presented in Fig. 1. We observe different peaks corresponding to different recombination processes. The emission lines are numbered, starting from high energy peaks with a descending order of energy. These emission lines are listed in Table I.

In the band edge region, some emission lines are due to the presence of impurities or native defects in the semiconductor material. In the literature, several studies have been carried out on these acceptors and donors in CdTe (see Annex A). However, based on the spectrum shown in Fig. 3, the recombination lines cannot be associated with contaminants or native defects with certainty. Concerning the $A^{\circ}X$ peaks, it is unclear whether lithium, sodium [15] or intrinsic defects [16] are responsible for these emissions, since their respective published

positions are very close to each other. Similar conclusions hold for the $D^\circ X$ peaks. It is not obvious to identify from the broad $D^\circ X$ peak, the chemical species that are present in the material.

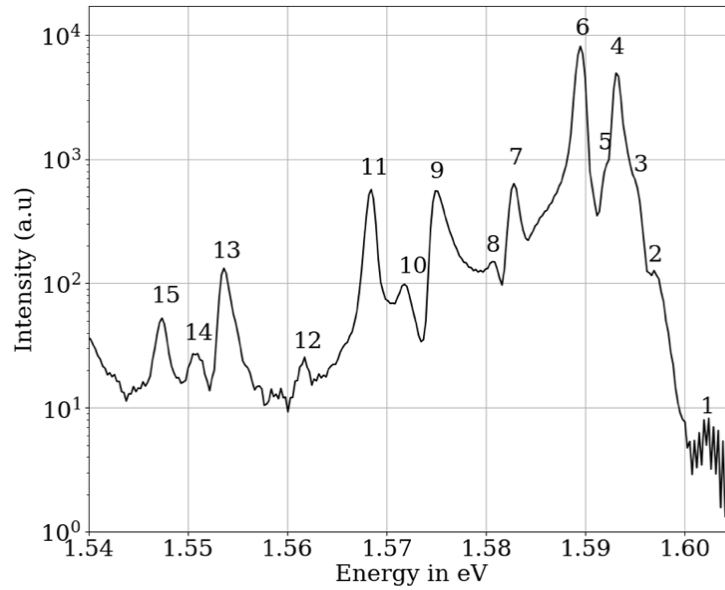


Fig. 3 – Measured band edge photoluminescence spectrum of CdTe at 4 K (log scale).

Table 2 - Energies of emission lines corresponding to excitonic recombinations in CdTe observed at 4 K

Peak number	Energy in eV	Recombination process	Reference
1	1.6026	FX (n=2)	[17]
2	1.5969	X_L	[18]
3	1.5950	X_T	[18]
4	1.5931	$D_1^\circ X$	[19]
5	1.5921	$D_2^\circ X$	[20][16]
6	1.5896	$A_1^\circ X$	[21][15]
7	1.5828	$A_2^\circ X$	[22]
8	1.5806	FX (n=2)-1LO	
9	1.5749	FX-1LO	
10	1.5718	$D_{1-2}X$ -1LO	
11	1.5685	A_1X -1LO	
12	1.5618	A_2X -1LO	
13	1.5536	FX-2LO	
14	1.5508	$D_{1-2}X$ -2LO	
15	1.5475	A_1X -2LO	

The band-edge emission spectra of the two CdZnTe samples are plotted in log scale on Fig. 4 (it is a zoom of CdZnTe spectra shown in Fig. 1 on the corresponding emission region). As it was the case for CdTe semiconductor material, the band-edge emission regions of CdZnTe samples are constituted of bound and free exciton annihilations. The notations adopted to describe CdZnTe PL spectra are identical to those previously introduced for the CdTe PL spectra analysis. As both CdTe and CdZnTe samples come from the same foundry, it is possible to identify the emission peaks observed in the ternary alloys by analogy. The emissions lines are numbered and listed in Table 3. In each sample, the band edge emission region shows the same features as the CdTe sample. However, the $A^\circ X$ emission band (emission line number 4) is rather broad and may encompass emission from different kind of impurities. This broadening may be attributed to statistical fluctuations in the zinc concentration in the alloys [14]. In this emission region, the only difference between the two CdZnTe samples relies on the relative intensity of the $A^\circ X$ and $D^\circ X$ emission lines. Whereas, the second phonon replica of bound excitons are

visible on the PL spectrum of the CdTe sample (lines number 13, 14 and 15), these are not observed in the PL spectra of the CdZnTe samples.

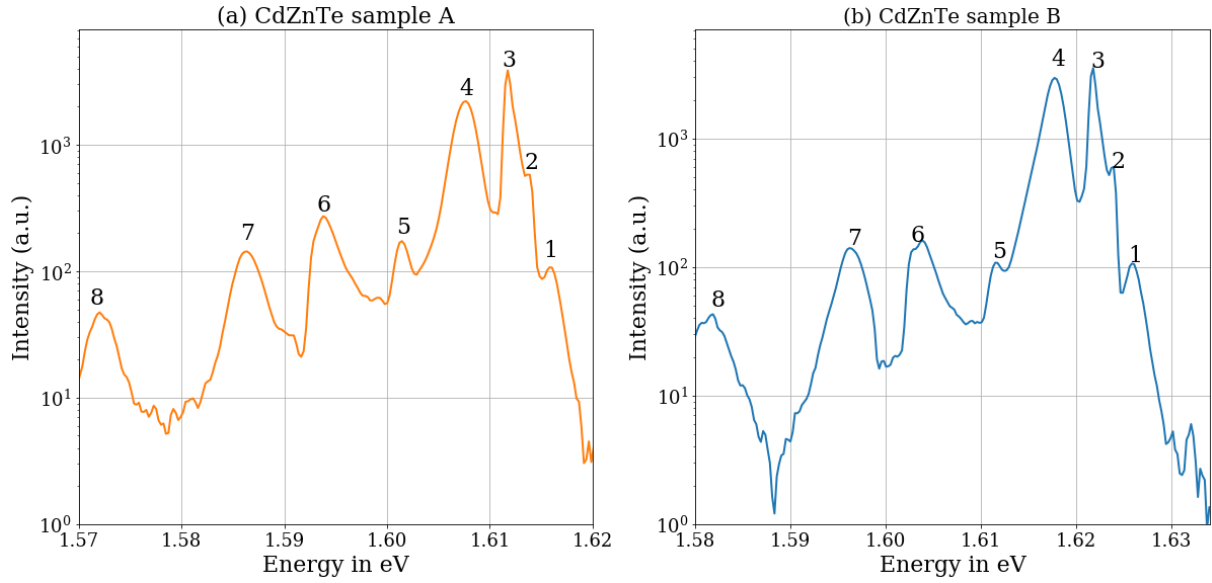


Fig. 4 - Measured band-edge photoluminescence spectra of the CdZnTe samples at 4 K (log scale). On the right, it is the CdZnTe sample A and CdZnTe sample B is reported on the left.

Table 3 - Energies of emission lines corresponding to excitonic recombinations in CdZnTe spectra (samples A and B) observed at 4 K in Fig. 4.

Peak Number	Energy in eV	Recombination process	Energy in eV	Recombination process
	CdZnTe A		CdZnTe B	
1	1.6158	X _L	1.6256	X _L
2	1.6138	X _T	1.6239	X _T
3	1.6118	D°X	1.6218	D°X
4	1.6076	A ₁ °X	1.6177	A ₁ °X
5	1.6015	A ₂ °X	1.6115	A ₂ °X
6	1.5938	FX-1LO	1.6039	FX-1LO
7	1.5905	DX -1LO	1.5962	AX-1LO
8	1.5749	AX-1LO	1.5820	FX-2LO
9	1.5718	FX-2LO		

In the following, we will first focus on FX recombination in CdZnTe and CdTe samples in the temperature range 4 K to 50 K, before concentrating on bound exciton recombination.

In the CdTe sample, as can be seen on **Fig. 3**, the energy of the ground state corresponding to FX annihilation is hardly resolvable on the photoluminescence spectra. Hence, the emission line corresponding to the FX recombination was determined relying on the position of its first phonon replica (emission line number 8) as expressed by Eq. (1). Considering that the phonon energy in the CdTe is equal to 21.3 meV [15], [18], [20],[23], taking into account the average kinetic energy of the exciton involved in the recombination, which is equal to 0.57 meV at 4 K, one can estimate the exciton energy in CdTe equal to 1.5960 eV. Adding the binding energy of the exciton, E_x , which is equal to 10.6 meV [24] (10.5 meV [25], 10.1 meV [25] and 10 meV [17], [26] energies were also reported), gives a bandgap energy of 1.6061 eV, according to Eq.(1). This value is very close to the well accepted value of 1.606 ([17] and references therein) of the CdTe energy gap at 4 K.

$$E_g = E_{FX-1LO} + E_{phonon} + E_x - E_{kinetic} \quad (1)$$

In CdZnTe sample A, excitonic recombinations lie on the energy range 1.6138 eV -1.6158 eV at 4 K. They lie at a slightly higher energy in sample B, 1.6239 eV – 1.6256 eV. The split between polariton branches, X_L and X_T , is equal to 2 meV in sample A and 1.7 meV in sample B, which is in good agreement with what was found by [18]. Regarding the localization of the FX, the same observation holds for CdTe and CdZnTe. Consequently, the FX energy was calculated from phonon-related recombinations. Since the amount of zinc in the alloys is low, the exciton binding energy and the phonon energy are assumed to be equal to the ones of CdTe, that is to say 10.6 meV and 21.3 meV respectively. From these considerations, since the energy of the FX-1LO is equal to 1.5938 at 4 K, the energy of the FX in sample A is equal to 1.6157 (taking into account the kinetic energy of the exciton at 4 K). Adding the exciton binding energy leads to 1.6253 eV for the bandgap at 4 K of the CdZnTe sample A. The difference between the bandgap energies of CdTe and CdZnTe at 4K is equal to 19.2 meV. Similarly, one can derive the bandgap value of the CdZnTe sample B, which was evaluated to be equal to 1.6354 eV. This is 29.3 meV higher than the CdTe bandgap value.

Different formulas [14], [27]–[29] have been published to express the bandgap energy of the CdZnTe ternary alloy as a function of zinc composition at low temperature. The expression of Tobin et al. [27] is the most widely used and is valid at 4 K for a zinc concentration between 3 % and 6 % (reported here by Eq. (2)). Hence, knowing the bandgap energy at low temperature, the amount of zinc in sample A can be deduced. It has been estimated to be equal to 3.6 %. This is in good agreement with the expected amount of zinc of 4 %. Whereas, the amount of zinc in the alloy B has been estimated to be equal to 5.5 % from Eq. (2).

$E_g(x) = 1.6058 + 0.546 x$	(2)
-----------------------------	-----

As already mentioned, different bound exciton recombinations are visible in the three samples (see **Fig. 3** and **Fig. 4**). However, clear identifications of the nature of the impurities or native defects involved in these deexcitation mechanisms is not possible, since the spectral resolution is not high enough and broad bands may encompass different kind of impurities. Nonetheless, it remains possible to calculate their energy of localization from Eq. (3), which states that the bound exciton recombination line is equal to the bandgap energy, E_g ; minus the exciton binding energy, E_x , and minus the energy of localization, E_{loc} .

$E = E_g - E_x - E_{loc}$	(3)
---------------------------	-----

The exciton energy of localization on donors and acceptors observed in the band-edge emission region in the different samples are reported in Table 4. These values have been calculated with energy values extracted from PL spectra at 4 K in each samples.

Table 4 - Value of exciton energy of localization on acceptors and donors

	CdTe		CdZnTe sample A		CdZnTe sample B	
	Peak number	E_{loc} in meV	Peak number	E_{loc} in meV	Peak number	E_{loc} in meV
<i>Donor exciton localization energy</i>	4	2.4	3	2.9	3	3.0
	5	3.4				
<i>Acceptor exciton localization energy</i>	6	5.9	4	7.1	4	7.1
	7	12.7	5	13.2	5	13.3

Whereas, the donor exciton localization energies are close in CdTe and CdZnTe material, which suggest identical impurities, the acceptor exciton localization energies are different in CdTe and CdZnTe samples. However, the acceptor localization of energies are equal in the two CdZnTe samples.

In the literature, a specific emission line around 24 meV below the conduction band was reported for CdZnTe by Hjelt et al. [22]. It was suspected to be linked to the recombination of exciton bound to a deep acceptor complex formed with Cd vacancies (noted V_{Cd}). In CdZnTe sample A and B, emission line number 5 lies 23.8 meV and 23.0 meV below the bandgap respectively. These values are very close to the one of [22], which may suggest that the acceptor A_2 is a deep acceptor formed with V_{Cd} . In CdTe, the emission line (at 1.5828 eV at 4 K) is not clearly identified and seldomly mentioned in the literature for CdTe material. However, since it is located 23.3 meV below the bandgap, we associate this emission lines to the same mechanism.

At 4 K, in CdTe and CdZnTe B, the band-edge emission region of the PL spectrum is dominated by the annihilation of excitons bounded to acceptors. As the temperature increases, $D^{\circ}X$ contributions intensify and finally dominate the PL spectrum. In CdZnTe A, the $D^{\circ}X$ recombination process dominates at 4 K and remains the main source of emission with increasing temperature.

b) Study of middle energy range (1.47 eV – 1.54 eV) of CdTe and CdZnTe samples from 4 K to 50 K

The CdTe PL spectrum at 4 K is shown on **Fig. 1**, represented by the blue curve. For this specific temperature, a Donor Acceptor Pair (DAP) transition and its phonon replicas can be clearly identified and are shown on Fig. 5. A band to acceptor transition (eA°) can also be noticed, with its first's phonon replicas ($eA^\circ-1LO$ and $eA^\circ-2LO$). The PL spectra for higher temperatures (up to 50K) are plotted on the same figure. These particular emission peaks remain visible up to 50 K.

The DAP emission region of the CdZnTe sample A and B are plotted on Fig 5. The blue curves represent the PL spectra at 4 K. PL spectra at higher temperatures are also plotted on the same figure. One can notice that the shape of the DAP region is different in the two samples. The shape of this emission region in CdZnTe sample B is similar to the one of the CdTe reference sample. This suggests that the quality of CdZnTe sample B is better than the one of CdZnTe sample A, which is expected since CdZnTe sample B presents less second order defects than sample A.

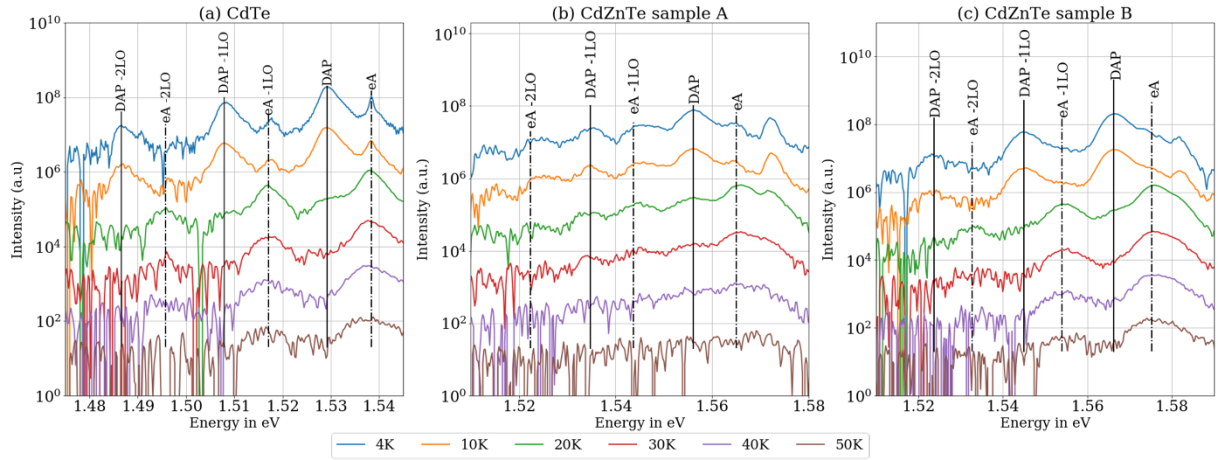


Fig. 5 - Thermal evolution of the the Donor Acceptor Pair (DAP) emission region of PL spectra of the CdTe sample and CdZnTe sample A and B. Spectra are shifted for clarity.

The evolution with the temperature of the CdTe eA° and DAP peaks' intensities are visible on Fig. 5 (a). It can be seen on this figure that at 4 K, the DAP recombination is the most intense. As the temperature increases, the eA° line intensifies as the donor involved in the DAP is being ionized. This phenomenon was also observed by other groups [20],[26][16]. Thermal evolution of the DAP emission region in the CdZnTe PL spectra are similar in the two samples, the DAP emission lines intensity decrease in the benefit of the eA recombination process.

As can be estimated from Fig. 5, the difference in energy of these two emission peaks, E_{DAP} and E_{eA} , is equal to 9 meV in the case of CdTe, thus giving the activation energy of the donor implicated in the DAP recombination (if we assume that the mean distance between donors and acceptors involved in the DAP recombination is large). Similarly, considering the two CdZnTe samples, the activation energy of the donor, E_D , can be calculated. The results are reported in Table 5. The activation energy of the donor in the three samples are very close, which may suggest that the donors are identical.

Moreover, given the position of the eA° emission peak at a specific temperature, one can calculate the value of the acceptor activation energy, E_A , using Eq. (4) [30], where E_g is the bandgap, k_B is the Boltzmann constant and T_e is the effective temperature of electrons in the conduction band. It is assumed here that the electron effective temperature is equal to the crystal lattice temperature.

$E_{eA} = E_g - E_A + \frac{1}{2} k_B T_e \quad (4)$
--

Let's consider first the CdTe sample. From the spectrum acquired at 4K in Fig. 2, considering a bandgap energy of 1.606 eV, the activation energy calculated is $E_A = 67.7$ meV. This energy is close to the activation energies of antimony and phosphate (respectively 65 meV and 68.2 meV as reported by Molva et al. [31]). However, we cannot firmly associate one of these impurities with the acceptor observed on Fig. 2. The donor and acceptor activation energies calculated here, respectively 9 meV and 67.7 meV, are different than those determined by Lee et al. ($E_A=56.4$ meV, $E_D=7$ meV) [20] and Shin et al. ($E_A=56.4$ meV, $E_D=7$ meV) [16] in CdTe crystals.

The band to acceptor recombination observed in the case of CdTe is not clearly visible in the CdZnTe samples A and B at 4 K. As it lies in the region where the $A_1^\circ X - 2LO$ emission should occur, these two lines are probably merged. Nonetheless, the activation energies of the donor and the acceptor involved in the DAP recombination in the two CdZnTe samples, A and B, have been derived with the same method. The values are reported in Table 5. The acceptor activation energies in CdZnTe samples are close to Na one which is equal to 58.7 meV in CdTe [15]. Whereas E_A values are close in CdZnTe sample A and B, they are lower than the one calculated from the CdTe PL spectrum, but they are similar to the ones determined by Gemain [26]. In the latter study, the acceptor is unidentified, and the donor is suspected to be linked to alkali atoms on interstitial sites.

Table 5 - Value ionization energy of the donor and the acceptor involved in the DAP recombination mechanism in CdTe and CdZnTe samples.

	CdTe	CdZnTe sample A	CdZnTe sample B
E_A	67.7 meV	60.7 meV	60 meV
E_D	9.0 meV	8.8 meV	9.1 meV

In this section, the DAP emission region has been studied. Activation energies of donors and acceptors have been calculated in the three samples. Furthermore, thermal evolution of the DAP and eA° emission lines have been analyzed. The next section focuses on the deep emission region in each sample.

c) Study of deep emission region at 4K

In the literature two bands were observed in the deep emission region: the first one centered around 1.4 eV and the second one centered around 1.1 eV.

The 1.4 eV band was widely studied [32]. It was associated with the formation of a complex composed of a native defect (a V_{Cd}) and a shallow donor [32]. It is known as the ‘‘A-center’’. The formation of this complex was observed for different donors such as In, Cl and Ga [33]. However, Krustok et al. [34] pointed out that this band may be composed of at least 3 sub-bands, originating from different type of defects. Close to this 1.4 eV band, another band (sometimes called Y) is also mentioned in the literature with a Zero Phonon Line (ZPL) at 1.475 eV. This band was observed in CdTe samples doped with iron by Lischka et al. [35]. Whereas Kuciauskas et al. [36] associate this emission line with the recombination of excitons bound to extended defects which is suspected to be due to slip dislocations [37][38]. This 1.4 eV band is not very intense on the CdTe PL spectrum plotted on Fig. 6. It is orders of magnitude weaker than the band edge region.

A weak emission feature is visible on the CdZnTe sample A and B. This emission region is plotted on Fig. 6. The PL signal is weak and barely rises above the noise. The maximum of emission of the deep region in the CdZnTe samples is 1000 times lower than the maximum emission at 4 K (which corresponds to the band-edge emission region). This band, centered at 1.44 eV and 1.45 eV in sample A and B respectively. Although this band of luminescence emission is very weak and represents only a fraction of the total intensity of emitted light, as we are dealing with highly sensitive IR detectors, attention should be paid to this low light level emission. Indeed, the energy of these photons is below the bandgap energy of the CdZnTe, hence one could expect that they will be only weakly absorbed. Consequently, when the detectors will be submitted to proton irradiation, part of the luminescence photons will be emitted in this emission region in the CdZnTe substrate. These photons will propagate over long distances inside the substrate before being collected by the HgCdTe light sensitive layer and may pollute large areas of the detectors. Further cathodoluminescence measurements performed at 80 K and 100 K will show that this emission band remains visible in the CdTe sample and in the CdZnTe sample A.

At even lower photon energies, another emission band at 1.1 eV has been identified in the literature. Lischka et al. [35] correlate this band with the presence of iron in the sample. Whereas Castaldini et al. [39] identify it to be related to telluride vacancies. However, on the Fig. 6, this band is not very intense on our samples, and barely rise above the noise, hence this emission band was not further studied.

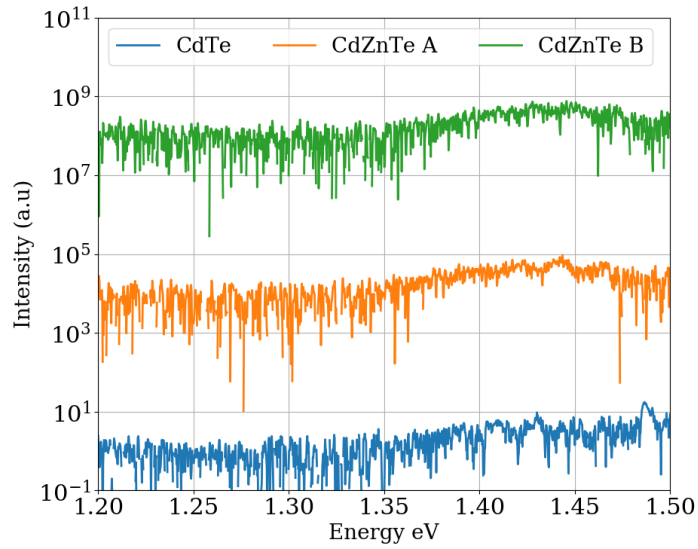


Fig. 6 - Deep emission region of PL spectrum for CdTe and CdZnTe samples at 4 K

3- Summary of PL measurements

The measured exciton localization energy as well as the activation energy of our samples are presented on Table 6. As can be seen on the table, the energy of localization of donors in both CdTe and CdZnTe (sample A and B) are similar. The acceptors are probably different in the binary and ternary alloys, since exciton localization energy and acceptor activation energy are different. Only the acceptor with a strong energy of localization (12.7 meV) is probably present in the three samples. This acceptor was associated to complexes formed with V_{Cd} [22]. In each sample, the deep band emission region was visible at 4 K, although it remains very weak.

Table 6 - Summary of bandgap value at 4K, exciton energy of localization, activation energy, and deep band emission characteristic

	CdTe	CdZnTe sample A	CdZnTe sample B
E_g at 4 K	1.6061	1.6253	1.6354
Donor exciton localization energy	2.4 meV 3.4 meV	2.9 meV	3.0 meV
Acceptor exciton localization energy	5.9 meV 12.7 meV	7.1 meV 13.2 meV	7.1 meV 13.3 meV
E_A	67.7 meV	60.7 meV	60 meV
E_D	9.0 meV	8.8 meV	9.1 meV
Deep band	Very weak, centered at 1.42 eV	Very weak, centered at 1.44 eV	Very weak, centered at 1.45 eV

Photoluminescence spectra have been studied for the three samples. Three emission regions have been identified: the band edge emission region, the DAP emission region and the deep emission region. The latter has been observed in the three samples at 4 K and is of particular interest within our framework of study. Indeed, the main objective of this study is to determine the optical properties of CdZnTe samples when used as a substrate for HgCdTe based IR detectors. In particular, it is essential to know the luminescence properties of CdZnTe substrate in order to understand the effect of proton interactions with IR detector in a space environment. Near IR detectors are typically operated at 100 K. However, with our PL experimental set-up, above 50 K, the luminescence signal was too low to be measurable. Hence, we have performed cathodoluminescence (CL) measurements in order to obtain the luminescence properties of CdZnTe substrate.

An additional objective was to discriminate sample quality through PL measurements. It has been shown in the previous section that the band-edge emission region and the deep emission region are identical in the two CdZnTe crystals. The shape of the DAP emission was the only difference between CdZnTe A and B, which may suggest that DAP emission region is a marker of crystal quality.

In the next section, the CL spectra of the three samples at 300 K, 100 K and 80 K are presented and analyzed.

iv – Cathodoluminescence spectrum measurement

1- Experimental Set Up for cathodoluminescence measurement

Cathodoluminescence (CL) measurements were performed for the same three samples (CdTe, CdZnTe Sample A and CdZnTe Sample B) at four different temperatures (300 K, 100 K, 80 K) using a dedicated test bench. Experiments were carried out using an Attolight commercial Rosa CL setup allowing for hyperspectral imaging. The electron beam acceleration voltage is 10 keV, with a beam current of 25 nA. The light is collected using a Cassegrain-type objective (NA 0.72) embedded inside the electronic column of the scanning electron microscope. The collected light is focused on the entrance slit of a spectrometer (Horiba Jobin-Yvon IHR320), dispersed using a 150 gr/mm grating blazed at 500 nm, and detected using a CCD camera (Andor Newton).

2- CL spectra of CdTe and CdZnTe samples

a) CL spectrum of CdTe and CdZnTe samples at room temperature

The obtained CL spectrum at room temperature (RT) for CdTe crystal is plotted on Fig. 7. The CL spectrum is composed of a unique broad emission band, with an asymmetrical shape. The energy corresponding to the maximum emission is equal to 1.507 eV, which is 6 meV under the most commonly used CdTe energy bandgap at RT (1.513 eV) [23]. As can be noticed on the figure, no significant signal is visible at lower and higher energies.

Li et al. [40] suggest to determine the bandgap energy of a semiconductor material from its luminescence spectrum, by adjusting experimental data to a model of light emission. This model assumes a band to band radiative recombination. When considering a semiconductor with parabolic bands (which to some extent is the case for CdTe and CdZnTe materials [40]), the luminescence intensity for an ideal crystal, can be modelled by Eq.(5). In this equation I_{PL}^+ is the light intensity when considering band to band transition, $\hbar\omega$ is the energy of the emitted photon, E_g is the bandgap energy of the material, T_e is the effective temperature of the material,

$$I_{PL}^+(\hbar\omega) = \begin{cases} A(\hbar\omega)^2(\hbar\omega - E_g)^{\frac{1}{2}} \exp\left(-\frac{\hbar\omega - E_g}{k_B T_e}\right) & \text{if } \hbar\omega > E_t \\ 0 & \text{if } \hbar\omega < E_t \end{cases} \quad (5)$$

k_B is the Boltzmann constant, A is a proportionality parameter. According to Eq. (5), luminescence intensity should be equal to zero for an energy lower than the transition energy E_t . However, at room temperature, there is always light emitted with energy lower than the bandgap energy [30]. This can be explained by the existence of states close to the band-edges induced by fluctuations in the semi-conductor stoichiometry, or by defaults (impurity, native defects...) or linked to bound excitons. These shallow states in the bandgap gap are suspected to be at the origin of the Urbach tail [41], observed close to the optical absorption edge of semi-conductors. The light intensity corresponding to the emission of these photons is expressed by Eq. (6) [40].

$$I_{PL}^-(\hbar\omega) = \begin{cases} 0 & \text{if } \hbar\omega > E_t \\ \frac{N_e}{E_o} \exp\left(\frac{\hbar\omega - E_g}{E_o}\right) & \text{if } \hbar\omega < E_t \end{cases} \quad (6)$$

In this equation, I_{PL}^- is the intensity of the light emitted by defect related recombination, N_e is a parameter proportional to the density of states. Eventually, the luminescence spectrum of a semiconductor is expressed as the sum of Eq. (5) and Eq. (6), see Eq. (7), assuming band to band transition to be the main recombination process.

$$I_{PL}(\hbar\omega) = I_{PL}^+(\hbar\omega) + I_{PL}^-(\hbar\omega) \quad (7)$$

In this expression, A , E_g , T_e , N_e , E_t and E_0 are fitting parameters. The fit was performed using a least square method and is shown on Fig. 7.

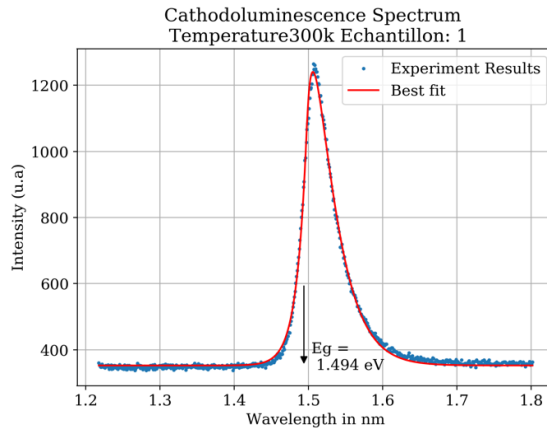


Fig. 7 – Measured cathodoluminescence spectrum for CdTe at 300 K superimposed to a modelled spectrum

With this method the bandgap energy of the CdTe material was determined to be equal to 1.494 eV, which corresponds to the bandgap energy as calculated by Li et al. [40] with the same method. This value lies in the range of bandgap energy mentioned in the literature which goes from 1.37 eV to 1.54 eV [17]. This bandgap energy will be further compared to the bandgap value inferred from other ellipsometry measurements in the next section.

As already mentioned, the model used to compute the bandgap energy assumes a band to band recombination process. However, Lee et al. [23] argued that the RT luminescence spectrum of CdTe material is mainly related to exciton recombination mechanism, by stating that the maximum of emission lies below the most commonly used bandgap energy value of 1.513 eV. In that case, if exciton-related emissions are the dominant recombination process, the model would not be applicable anymore. The nature of the luminescence at RT of CdTe material is still discussed.

In the following, the CL spectra of the two CdZnTe samples measured at room temperature are presented and discussed. The two spectra are plotted on Fig. 8. It can be noticed on the figure that the shapes of the spectra are similar. Similarly to what was done in the case of the CdTe sample, room temperature cathodoluminescence spectra are fitted according to the model of Li et al. [40], see Eq. (7). The energies of the maximum of emission lie at 1.528 eV and 1.536 eV for sample A and B respectively. This difference is explained by the difference in the amount of zinc in the alloys.

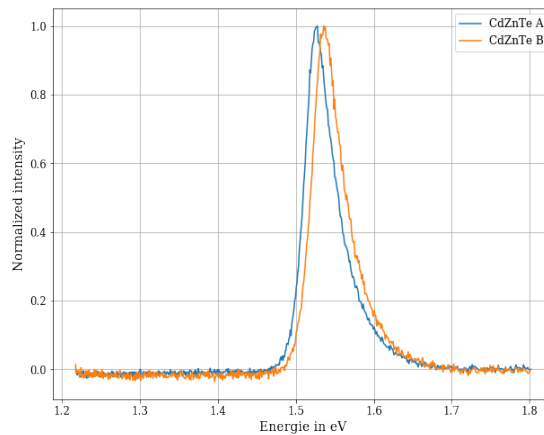


Fig. 8 – Measured cathodoluminescence spectra at room temperature of CdZnTe sample A and B

For both samples, the bandgap energies extracted from the fitting procedure are given in Table 7. Several formulas expressing the bandgap energy as a function of zinc concentration at room temperature have been proposed in the literature [14], [27], [42]. The obtained values using these formulas are listed in Table 7, for the amount of zinc previously determined at 4 K for both CdZnTe samples (3.6% for sample A and 5.5% for sample B). The bandgap energy derived from Johnson's expression [30] seems to underestimate the energy of the forbidden energy band compared to the other expressions. Tobin et al. [27] and Bouarissa [42] expressions are in good agreement.

At 4 K, we have calculated the difference between the bandgap energy at low temperature of the CdTe sample with the bandgap values of the CdZnTe samples. This difference is equal to 19.6 meV and 29.3 meV for sample A and sample B, respectively. The difference between the energy associated with the CL maximum emission at room temperature between CdTe and CdZnTe samples is equal to 21 meV, for sample A, and 29 meV, for sample B. This result is consistent with the differences calculated at 4 K.

Hence, we can assume that this difference remains almost constant over the temperature range 4 K – 300 K [18]. Thus, one can predict the value of the energy gap at room temperature for the two CdZnTe samples by adding this difference to the most commonly used value of $E_g(300\text{ K}) = 1.513\text{ eV}$ for the CdTe material (see Table 7). The energies derived are in good agreement with the bandgap energies calculated with the expression of Olego et al. [14]. Since the CL maximum of emission is lower than the bandgap energy, following the argument of Lee et al. [23], this seems to suggest that the main recombination process in these samples at room temperature is not related to band-to-band transitions, but is probably excitonic.

Table 7 - Bandgap energies extracted from measured CL spectra or calculated for the two CdZnTe samples using formulas from the literature at 300 K

	CdZnTe sample A	CdZnTe sample B
<i>Maximum of emission on the measured CL spectrum</i>	1.528 eV	1.536 eV
<i>Extracted from fit of the measured CL spectrum [40]</i>	1.512 eV	1.522 eV
<i>Estimated from Tobin formula [27]</i>	1.527 eV	1.540 eV
<i>Estimated from Bouarissa formula [42]</i>	1.527 eV	1.539 eV
<i>Estimated from Olego formula [14]</i>	1.531 eV	1.544 eV
<i>Estimated from Johnson formula [27]</i>	1.481 eV	1.492 eV
<i>Extrapolated from CdTe bandgap energy at 300 K</i>	1.533 eV	1.543 eV

b) CL spectrum of CdTe and CdZnTe samples at 80 K and 100 K

Cathodoluminescence measurements were also performed at 100 K and 80 K on the three samples. As a reminder, 100 K is the operating temperature of the short-wave IR detectors in the astrophysics domain. And 80 K corresponds to the thermal operating conditions of IR detectors irradiated during an irradiation campaign. Hence, the luminescence spectra acquired at these 2 temperatures are of primary importance since they will give insight into the energy of the photons emitted through radiative recombination. If we assume that recombination mechanism are independent of the source of excitation (either electrons or protons), these spectra will give the energy of the photons emitted by deexcitation of carriers inside the CdZnTe substrate of HgCdTe-based IR detectors.

The measured spectra of the CdTe sample at 80 K and 100 K are represented on Fig. 9. It can be seen on the figure that for each temperature the spectrum is dominated by a broad band. At 80 K, the maximum of emission lies at 1.580 eV, which is below the bandgap energy values mentioned in the literature, ranging from 1.590 eV to 1.607 eV [17], [43]–[47]. On the figure, one can notice a very weak emission band around 1.4 eV, 150 times less intense than the main emission peak. This emission region has already been discussed in Section III.2.c. It represents less than 3 % of the total integrated intensity at 80 K. At 100 K, the spectrum presents the same features. A main broad line dominates the spectrum and the emission at 1.4 eV still exists but is weaker than in the 80 K case. The principal emission line is localized at 1.574 eV, which is below the bandgap values reported in the literature lying in the following energy range: 1.584 eV to 1.596 eV.

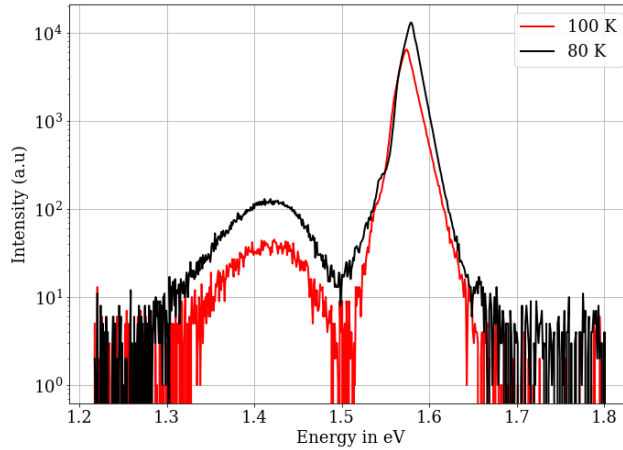


Fig. 9 – CL spectra at 80 K and 100 K of CdTe sample). Log scale.

The CL spectra of CdZnTe samples A and B were measured at 80 K and 100 K. The spectra are presented on Fig. 10. Only the CdZnTe sample A exhibits emission in the 1.4 eV. region, this band corresponds to the so-called A-center in the CdTe. This emission band was already discussed in a previous section III.2.c). However, the intensity of the band is still very weak compared to the main emission band (about 1 000 times lower) and represents less than 5 % of the total integrated intensity at 80 K. At this temperature, the maximum of emission is at 1.598 eV for sample A, and 1.609 eV for sample B. At 100 K, the shapes of the spectra are similar. The intensity of the mean peaks decreases of about few percent as well as that of the deep emission region. The positions of the maxima of emission are 1.593 eV and 1.604 eV, for sample A and sample B respectively. Again, the differences in energy between the CdTe main peak position and CdZnTe peak position at 80 K and 100 K are approximately equal to 20 meV and 30 meV, for sample A and sample B respectively.

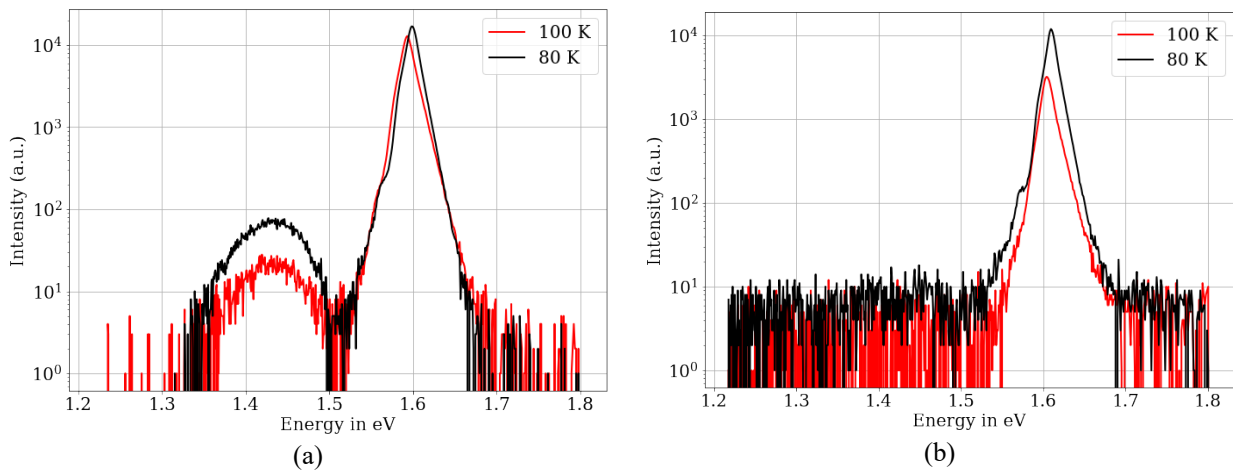


Fig. 10 – CL spectra at 80 K and 100 K of CdZnTe sample A on figure (a) and of CdZnTe sample B on figure (b). Log scale.

3- Summary of CL measurements

CL measurements have been performed in order to obtain the luminescence spectra of CdZnTe and CdTe samples. The main results of these measurements are reported on Table 8. The objective of this work is to determine the energy of the photons emitted by radiative recombination within the substrate at 80 K and 100 K (these temperatures are close to operating temperature of near IR detectors in the astrophysics domain). Under ionizing particles irradiation, electron-hole pairs are generated within the substrate of IR detector when not removed. They may recombine radiatively. The emitted photons are in turn detected by the light sensitive layer. We have seen thanks to CL spectra that depending on the sample quality, low energy photons will be emitted. These photons will be the most polluting since they will not be absorbed and may propagate over long distances. Consequently, crystal quality appears to be an important factor in order to mitigate the effect of energy deposition inside the substrate of HgCdTe based IR detectors.

Table 8 - Summary of values extracted from CL measurements on CdTe and CdZnTe samples

	CdTe	CdZnTe sample A	CdZnTe sample B
300K			
<i>Bandgap energy calculated from fit</i>	1.494 eV	1.512 eV	1.522 eV
<i>Peak emission</i>	1.507 eV	1.528 eV	1.536 eV
<i>Band at 1.4 eV</i>	No	No	No
100 K			
<i>Peak Emission</i>	1.574 eV	1.593 eV	1.604 eV
<i>Band at 1.4 eV</i>	Yes	Yes	No
80 K			
<i>Peak Emission</i>	1.580 eV	1.598 eV	1.609 eV
<i>Band at 1.4 eV</i>	Yes	Yes	No

In order to determine the optical losses due to propagation of photons emitted by radiative recombination within the substrate, the absorption coefficient should be determined. Consequently, we have performed ellipsometry measurement on CdTe sample and CdZnTe sample A. The optical properties of CdZnTe B were not measured, since we expect these to be very close to the one CdZnTe sample A. Moreover, as ellipsometry is a non-local method, we do not get insight into the crystal quality through ellipsometry measurements. The experimental set-up and the results are presented in the next section.

v – Ellipsometry measurements

1- Experimental set-up for ellipsometry measurements

In this study, in-situ spectroscopic ellipsometry (SE) measurements were performed at different temperatures, at angle of incidence of 70° . Woolam ellipsometer was used in this experiment. The sample was installed inside a dedicated cryostat. The temperature of the sample was monitored with a Lakeshore cryogenic temperature controller and could be tuned from 77 K to 500 K. The sample was cooled down using liquid Nitrogen. The incident light and the reflected light pass through glass windows which could induce uncertainties in the estimation of the optical parameters. Another source of error is linked to the position of the sample, which can be slightly tilted. Thus, exact determination of the incident angle is hardly achievable regarding our experimental set up. An error estimation on the measured optical properties was performed using a propagation error calculation (see Annex A). It takes into account two contributions: the uncertainty on the sample position and the cryostat window parasitic effects. A similar calculation was previously done in [48].

The ellipsometer was calibrated with a reference sample of SiO₂ at 300 K. During this calibration, retardances due to the windows were taken into account. As we go at low temperature or as we change from one sample to another, light does not cross the windows at the exact same position. Consequently, uncertainties on these parameters still exist. These errors are taken into account in the expression dN_1 (see Annex B). The uncertainty within the incident angle is chosen to be equal to 0.5° . This value has been estimated from the measurements made with the SiO₂ reference sample.

Before each measurement, the samples were plunged in an HCl bath, before being rinsed with deionized water to get rid of residual HCl. Rear surfaces were frosted in order to reduce the effect of back reflection on the rear surface of the samples. Measurements of the optical properties were performed at three different temperatures: 300 K, 100 K and 80 K.

2- Ellipsometry measurement for CdTe sample

For the CdTe sample, the measurements were performed in the energy range 1.25 eV - 3.00 eV. The obtained real and imaginary parts of the dielectric function ϵ_1 and ϵ_2 , respectively, measured at 300 K are shown on the **Fig. 11**. In the inset, a zoom is made around the bandgap energy of the material.

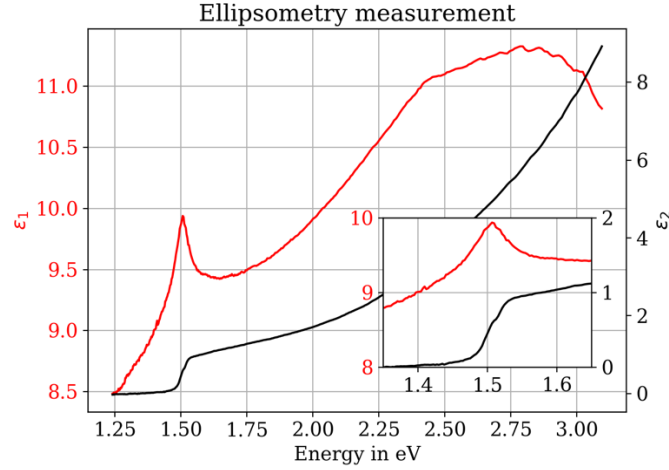


Fig. 11 – Measured real and imaginary parts of the dielectric function ϵ_1 and ϵ_2 , respectively, for CdTe at 300 K

The real and imaginary parts of the refractive index, $n(E)$ and $k(E)$ respectively, are related to the dielectric function by Eq. (12) and Eq. (13) [49].

$$n(E) = \frac{\sqrt{\epsilon_1(E)^2 + \epsilon_2(E)^2} + \epsilon_1(E)}{2} \quad (12)$$

$$k(E) = \frac{\sqrt{\epsilon_1(E)^2 + \epsilon_2(E)^2} - \epsilon_1(E)}{2} \quad (13)$$

The obtained real part of the refractive index is shown on **Fig. 12** (a), where it is superimposed to literature data based on the work of Adachi [50], Marple et al. [51], Hildek [52], and Finkman et al. [53]. As can be seen on the figure, the measured real part of the refractive index is higher than what was previously reported in the literature. This difference may be explained by the important uncertainty on the tilt of the sample, which in turn induces an uncertainty on the angle of incidence.

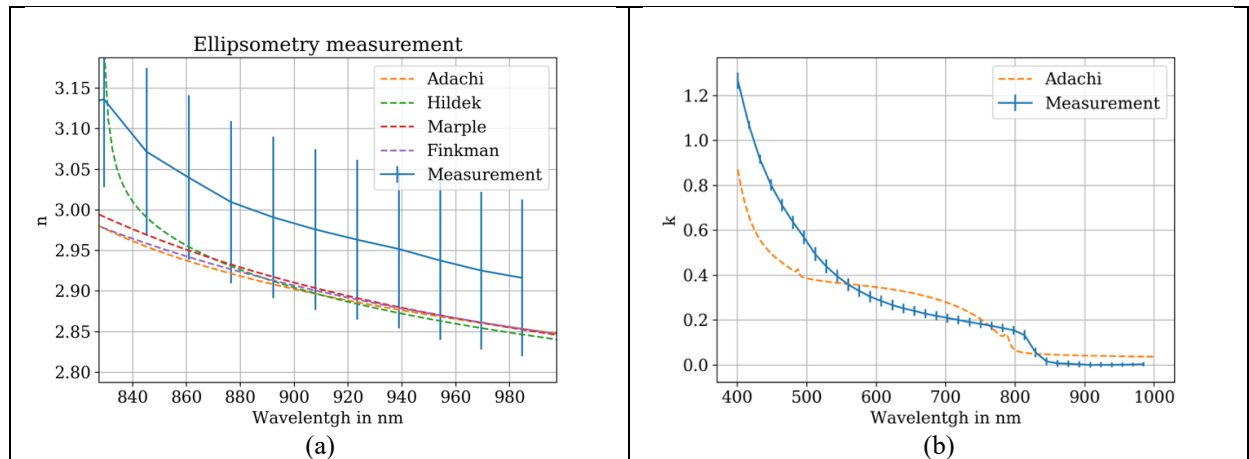


Fig. 12 – (a) Measured real part of the refractive index of CdTe at 300 K superimposed to literature data [50], [51], [53], [54]. (b) Measured imaginary part of the refractive index (extinction coefficient) of CdTe at 300 K superimposed to Adachi data [50].

The obtained imaginary part of the refractive index, also named extinction coefficient k , is shown on **Fig. 12** (b), where it is superimposed to measurement of Adachi [50]. It can be seen on the figure that there is a spectral shift between the two curves. This can be explained by the differences in the growing conditions of the CdTe material.

The bandgap energy was estimated using two methods: as an output of the fit performed by CompleteEASE software on the measured curves and by taking the maximum of the derivative of the extinction coefficient k , assuming band-to-band transition. The first method gives a bandgap energy of 1.500 eV whereas the second one gives a value of 1.498 eV at 300 K. These two energies are in fairly good agreement, they are reported in Table 8.

The measurements of the optical parameters were done at lower temperature 100 K and 80 K. The results of these measurements are shown on **Fig. 13**. Below 100 K, excitonic behavior of the semiconductor is observed. This is visible in the figure inset, where a small peak in the absorption coefficient is observed above the bandgap energy. This characteristic shape is associated with the exciton density of states which provides accessible states in the bandgap [30]. This was previously observed in CdTe by other authors Quijada et al. [55] and Horodysky et al. [25]. The latter performed transmittance measurements through micrometer thick CdTe samples from 4 K to 500 K. They observed this specific trace induced by the excitonic behavior of the semiconductor up to 200 K. They also concluded that the absorption edge line shape was dominated by FX up to room temperature.

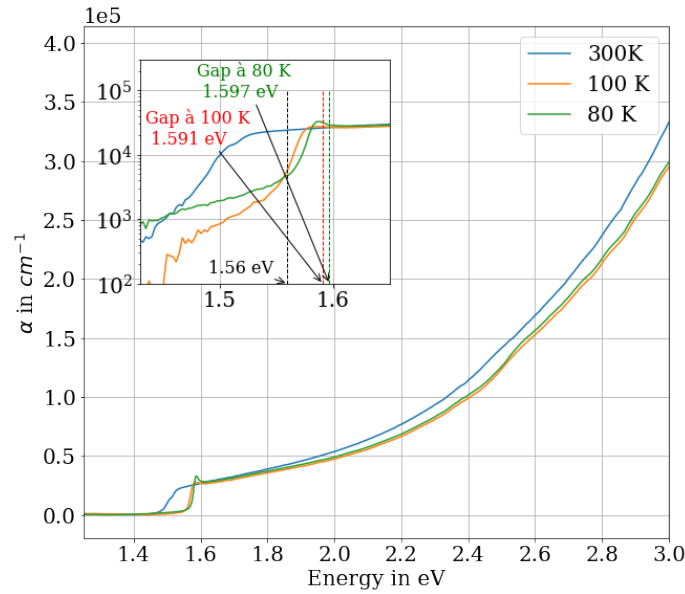


Fig. 13 – Absorption coefficient of CdTe measured from ellipsometry measurements at 300 K, 100 K and 80 K. In the inset a zoom is made on the energy range close to the bandgap. Excitonic behavior is visible on the absorption spectrum

Similarly to what was done at room temperature, the bandgap energy was estimated using the two methods previously described. However, the CompleteEASE fitting procedure does not take into account the excitonic behavior of the material, which may explain the difference between the two methods at 80 K and 100 K. Another method can be applied to calculate the bandgap energy at low temperature from the extinction coefficient spectrum. First, the exciton characteristic peak corresponding to the ground state of the exciton is localized, then the exciton binding energy, equal to 10.6 meV in the CdTe, (assumed to be independent of the temperature) is added. The results are given in Table 9.

Table 9 – Bandgap energy of CdTe at different temperatures, using several methods of estimation. 1st method: Complete EASE fitting procedure output. 2nd method: derivative of the extinction coefficient. 3rd method: excitonic absorption localization

	Method 1 – Fit	Method 2 - Derivative	Method 3 – Exciton Localization
300 K	1.500 eV	1.498 eV	-
100 K	1.563 eV	1.570 eV	1.5919 eV
80 K	1.567 eV	1.580 eV	1.5934 eV

3- Ellipsometry measurement for CdZnTe sample A

Ellipsometry measurement have been performed on CdZnTe sample A at 300 K, 100 K and 80 K. The measurements were done in the energy range 1.25 eV-3.00 eV. The refractive index has been computed from the real and imaginary part of the measured dielectric function. At room temperature, the refractive index, $n(E)$, and the extinction coefficient, $k(E)$ can be compared to the data of Adachi et al. [50] on Fig. 14. Similarly to the case of CdTe, we estimate the uncertainty in the angle of incidence to be equal to 0.5°. This value may be underestimated which could explain the difference between our measurements and the ones of Adachi et al. The

real and the imaginary parts of the refractive index are plotted on Fig. 14. However, this uncertainty in the angle of incidence does not explain the shift observed at the band-edge transition in Fig. 14. This was already seen in the case of the CdTe sample.

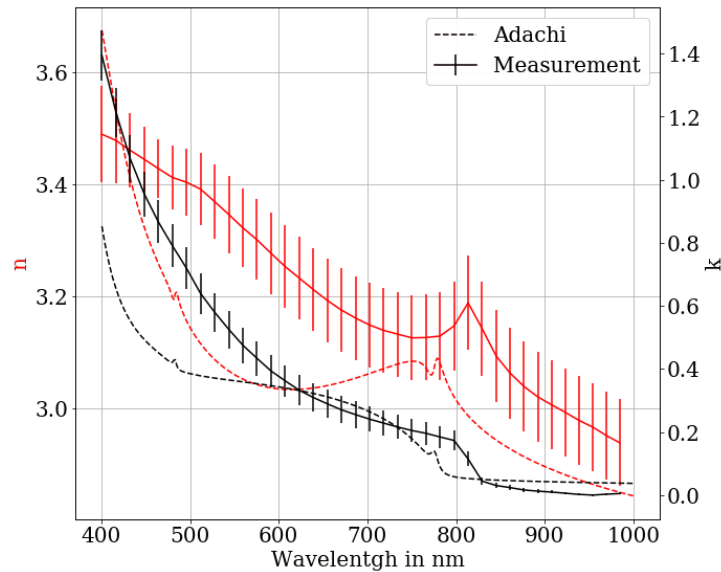


Fig. 14 - Real part of the refractive index at 300 K compare to the results of Adachi et al. on the CdZnTe sample A. Measured imaginary part of the refractive index (extinction coefficient) of CdTe at 300 K superimposed to Adachi data [50].

The absorption coefficient calculated from the ellipsometry measurement at 300 K, 100 K and 80 K are given in Fig. 15. The small increase in absorption after the rapid transition at 100 K and 80 K is a characteristic feature of excitonic absorption. This was already observed in the case of CdTe. The tail below the bandgap is more important in the case of the CdZnTe is more pronounced, which may be due to statistical fluctuations in the concentration of atoms in the alloy. Bad surface quality may also explain this important absorption below the bandgap, which is not expected.

In a similar way to what was done in the case of CdTe, one can derive the bandgap of the CdZnTe material through different methods at the three temperatures. The results are given in Table 10. The bandgap energy calculated at 300 K from the fit of the optical parameter with CompleteEASE software is in agreement with the bandgap value calculated from the fit of the CL spectra with Li et al. [40] formula, assuming band to band recombination. However, these two values are under the expected energy which is supposed to be equal to 1.533 eV, calculated from the CdTe bandgap value at 300 K.

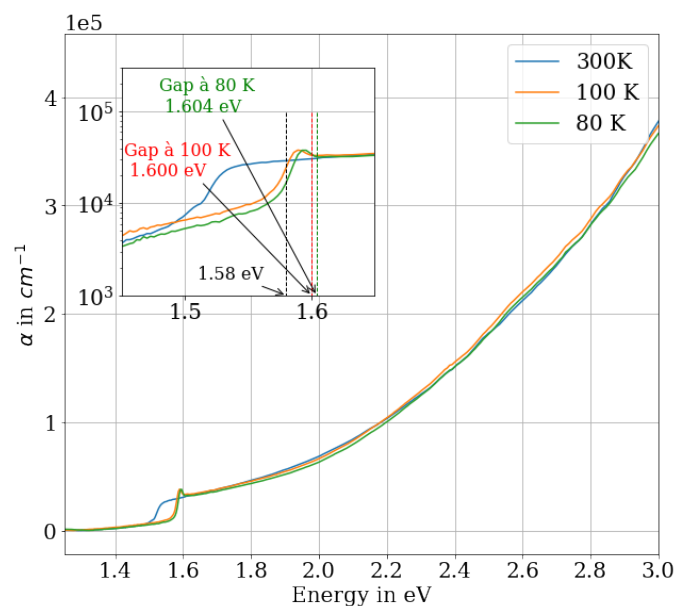


Fig. 15 – Measured absorption coefficient of the CdZnTe sample A, calculated from imaginary part of the refractive index at 300 K, 100 K and 80 K. In the inset, a zoom is made on the energy close to the bandgap.

Table 10 - Summary of Bandgap energy determination from the two methods. 1st Complete EASE fitting procedure output. 2nd method: derivative of the extinction coefficient. 3rd method: excitonic absorption localization.

	Method 1 – Fit	Method 2 - Derivative	Method 3 – Exciton Localization
300 K	1.518 eV	1.521 eV	-
100 K	1.571 eV	1.583 eV	1.600 eV
80 K	1.575 eV	1.586 eV	1.604 eV

4- Summary of ellipsometry measurements

Ellipsometry measurements were performed on CdTe sample and CdZnTe sample A and compared to data published in the literature. Below 100 K, excitonic behavior of the samples is observed. Moreover, the bandgap of the material was calculated at different temperature with different methods. Close to the CdTe and CdZnTe bandgap energy, the absorption coefficient is approximately equal to $2 \times 10^4 \text{ cm}^{-1}$. This value is within the order to magnitude expected for a direct bandgap semi-conductor [30]. This means that photons emitted at the band-edge by radiative recombination will strongly be absorbed and will not propagate over long distances in the CdZnTe substrate. In the last part, the different measurements done in this study are confronted and discussed. Detailed comparison of luminescence and absorption spectra is done, keeping in mind our initial problematic of image pollution in IR detectors under irradiation.

VI – Discussion

1- CdTe

The bandgap values of CdTe material at room temperature reported in the literature are overplotted with the bandgap calculated in this work in Fig. 16. The discrepancies found in the literature may be ascribed to different factors. For instance, the sample quality may be different or the methods used to calculate the bandgap energy may not be appropriate. However, the bandgap energy derived from our measurements is in good agreement with the values reported in the literature (see Fig. 16).

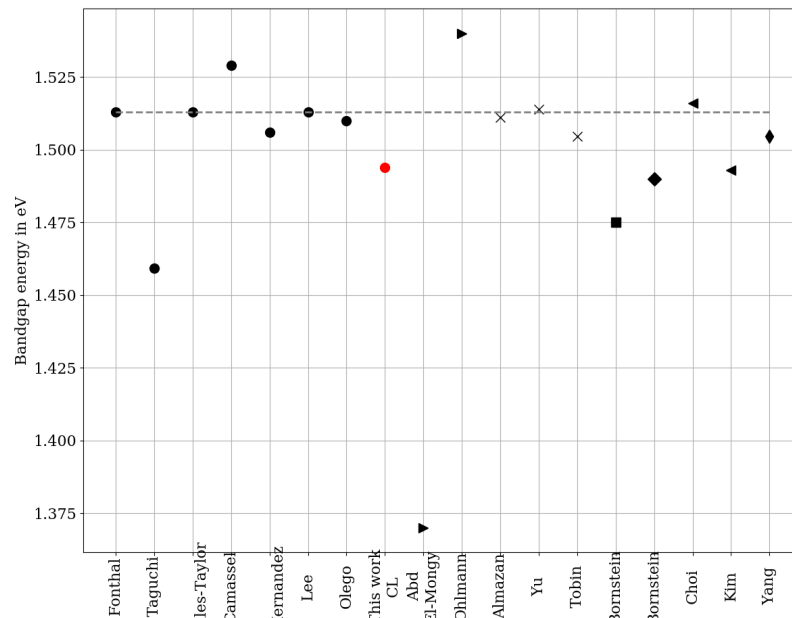


Fig. 16 - CdTe bandgap energy measured at room temperature superimposed to literature data. In red are reported the value are extracted from our measurements. The dashed line represents the most commonly used value in the literature, 1.513 eV [23]. ● refers to luminescence experiments, ► refers absorption experiments, × refers to photoreflectance measurements, ■ corresponds to electroreflectance measurements, ◆ photoelectrochemical experiment, ◀ absorption measurements, ◆ surface voltage spectroscopy.

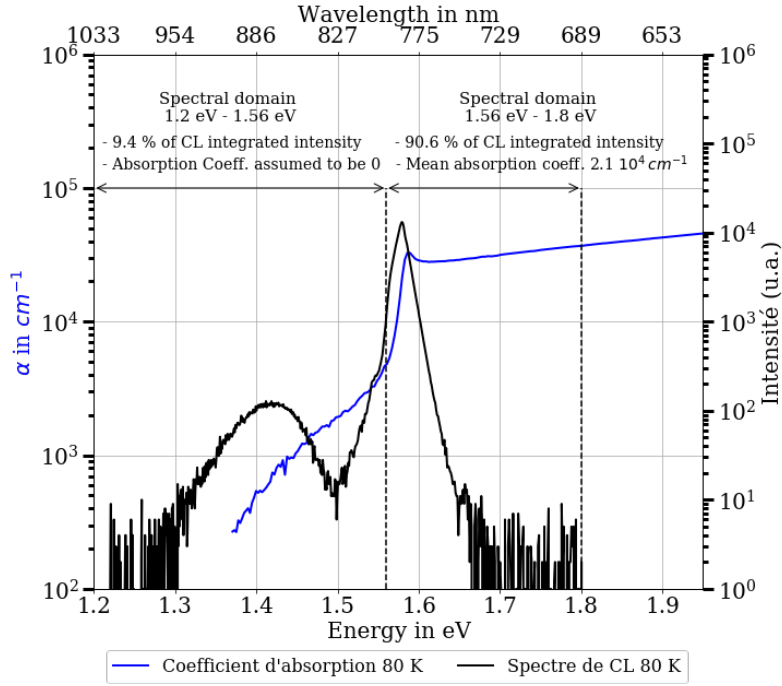


Fig. 17 - Plots of the CL spectrum and the absorption coefficient of the CdTe sample at 80 K measured in this work.

On Fig. 17, the absorption coefficient of the CdTe sample at 80 K is plotted in blue. On the same graph, the CL spectrum at the same temperature is shown in black. One can notice that the absorption coefficient is strong where the intensity of the CL spectrum is maximum and is equal to $3.2 \times 10^4 \text{ cm}^{-1}$. Which suggests that these luminescence photons will not propagate over long distances inside the CdZnTe substrate.

One can divide the CL spectrum in two regions. The first one encompasses 90.6 % of the total integrated intensity of the CL spectrum and corresponds to the region where the absorption is strong and is equal to $2.1 \times 10^4 \text{ cm}^{-1}$ over this spectral range. Hence, the propagation distance of the photons emitted in this spectral domain, defined as the inverse of the absorption coefficient, is very short and is equal to 470 nm. The second spectral domain corresponds to the emission region associated with the presence of defects inside the crystal, and represents 9.4 % of the total integrated intensity. This spectral range lies below the bandgap energy, where the absorption should be very low. But the absorption coefficient measured on the CdTe sample is important is this domain, which suggests that the absorption coefficient measured below the bandgap is over estimated. Regarding our problematic, this band of emission below the bandgap energy, yet very weak, can be at the origin of image pollution under irradiation.

2- CdZnTe samples

Over this study, we have noticed that the differences between the specific peaks of CdTe and CdZnTe remain almost constant over the whole temperature range. The difference in energy between CdZnTe sample A and CdTe is around 20 meV, while it is about 30 meV in the case of CdZnTe sample B. Hence, we propose a law to estimate the thermal evolution of bandgap energy of CdZnTe material with low zinc concentration (below 6%), given by Eq. (14).

$$E_g(x, T) = E_g^{CdTe}(T) + 0.545x \quad (14)$$

Where $E_g^{CdTe}(T)$ is the temperature evolution of the bandgap energy of CdTe, T is the temperature of the CdZnTe sample, and x is the zinc concentration within the sample. The amount of zinc within the CdZnTe material was calculated at low temperature with Tobin et al. formula (see Eq. (5)). The linear coefficient (0.545 eV) is very close to the one given in Tobin et al. expression [27] for the bandgap evolution of the CdZnTe as a function of the zinc concentration, which is equal to 0.546.

This work has been motivated by the need to determine optical parameters of CdZnTe material when used as a substrate for HgCdTe-based IR detectors. These parameters are then used to simulate the response of these IR detectors under irradiation. The photons emitted by radiative recombination of carriers generated by the passage of the proton are suspected to be at the origin of image pollution. On Fig. 18, the absorption coefficient and the CL spectrum of the CdZnTe sample A at 100 K are plotted. Similarly, to what was observed for the CdTe sample,

in the broad emission region, the absorption coefficient is strong whereas the photons emitted in the deep emission region, centered around the 1.43 eV will not be absorbed. Although this latter spectral region represents a small amount of the total integrated intensity of CL spectrum, the photon emitted in this spectral domain will be the most polluting regarding our study case. Indeed, they will be able to propagate over long distances inside the detector structure and pollute large areas. Nonetheless, in good quality samples (such as CdZnTe sample B) this 1.4 eV band is not observed (see Fig. 10 (b)). The photons emitted by radiative recombination are all emitted close to the band-edge emission region, where the absorption coefficient is strong. In a similar way to what was done for the CdTe sample, the CL spectrum will be divided in two regions as shown on Fig. 18. In the first spectral domain, the absorption is strong whereas the second emission region which represents 5.7 % presents a low absorption coefficient. The model has been validated experimentally using the optical properties of the CdZnTe sample measured in this work. The comparison between experiment and simulation has shown that detector image pollution under irradiation is attributed to the emission of low energy photons weakly absorbed in the CdZnTe substrate [13].

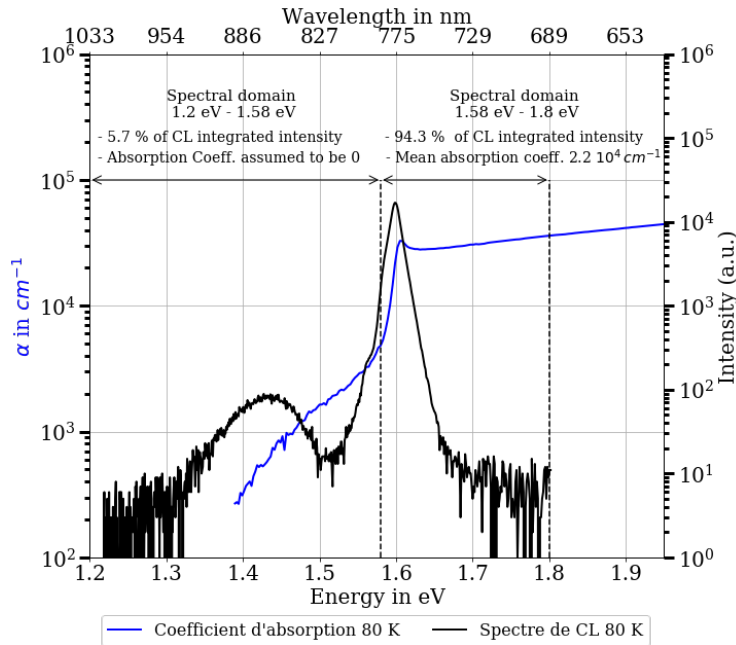


Fig. 18 - Plots of the CL spectrum and the absorption coefficient of the CdZnTe sample A at 80 K measured in this work.

VII – Conclusion

In this article, we have presented PL measurements from 4 K to 50 K of both CdZnTe and CdTe materials. It appeared that the corresponding spectra were highly similar. Cathodoluminescence spectra have also been presented and analyzed for different sample temperatures: 300 K, 100 K and 80 K. At 100 K and 80 K, the behavior of the semi-conductor appeared to be highly excitonic. Eventually, up to room temperature recombination process are related to excitonic mechanism.

Over this work we have noticed that the energy difference between CdTe and CdZnTe samples remain almost constant over the temperature range 4 K-300 K. This led us to propose a law for bandgap energy evolution of CdZnTe as a function of zinc composition. The expression is based on the knowledge of CdTe bandgap energy evolution with temperature. Moreover, we observed that Olego [14] formula, which expresses the bandgap energy value of CdZnTe material as a function of zinc composition, is in better agreement with our measurements at room temperature.

This study was motivated by the lack of literature data dealing with optical parameters of CdZnTe materials with low zinc concentration at 80 K and 100 K. In order to estimate the amount of pollution induced by luminescence of CdZnTe substrate on IR detectors, the energy of the photons and the absorption coefficient of the material are key parameters. It is now clear that, when excited, good quality Cd_{1-x}Zn_xTe material emits light only in a small energy band at 80 K or higher. In this emission region, the absorption coefficient is high. Hence the photons emitted by radiative recombination inside the semi-conductor will not travel far from their emission point and will be quickly absorbed. An emission region centered around 1.4 eV may still be visible up to 100 K. But this emission band is not visible on high quality samples (see results for CdZnTe sample A). Yet low energy photons represents the weakest luminescence contribution, the comparison between simulation and experiment has

shown it is the main source of pollution of IR detector images with thick CdZnTe under proton irradiation. In order to fully model luminescence phenomenon inside the CdZnTe substrate of HgCdTe based IR detectors, measurements of electrical parameter such as diffusion length and carrier lifetimes should also be done close at the operating temperature of the detectors.

Annex A

Review of bound exciton recombination's lines

Table I - Summary table of the energetic positions of lines related to acceptor impurities or acceptor defects in the PL spectrum of CdTe or CdZnTe. Data from the literature.

A°X (en eV) – Raie de PL	Impuretés identifiées	Référence
1.5896	Cu	Chamonal [21]
1.5885	Ag (sur un site de Cd)	Chamonal [21]
1.58848	Ag	Hamann [56]
1.58916	Na	Molva [15]
1.58923	Li	Molva [15]
1.58897	P	Molva [31]
1.57606	Au	Capper [57]
1.5892	N	Capper [24]
1.58970	As	Capper [24]
1.589	V_{Cd} -2D	Shin [16]
1.5896	$(V_{Cd}^{2-} - D^+)^-$	Seto [58]
1.589	V_{Cd}	Shin [16]

Table II – Summary table of the energy positions of lines related to donor impurities in the PL spectrum of CdTe or CdZnTe (data from the literature)

D°X (en eV) – Raie de PL	Impuretés identifiées	Référence
1.59309	Ga	Francou [19]
1.59302	In	Francou [19]
1.59296	Cl	Francou [19]
1.59314	F*	Francou [19]
1.59305	Al*	Francou [19]

Annex B

Propagation Error calculation

Spectroscopic ellipsometry measurements rely on the estimation of the ratio two reflection coefficients. One coefficient for each polarization state: r_p (p stands for *parallel*) and r_s (s stands for *senkrecht*, perpendicular in german). These values include the modification in phase and amplitude induced by the reflection of the light on the sample. This ratio is a complex value written as Eq. (1).

$$\rho = \tan(\psi) e^{i\Delta} = \frac{r_p}{r_s} \quad (1)$$

Δ is the phase shift between the two polarization induced by the reflection on the sample, and ψ holds for the difference between the two polarization amplitudes. The expressions of the reflexion coefficients are derived with the use of the continuity equations of the electric and the magnetic fields.

$$r_p = \frac{N_1 \cos(\phi_0) - N_0 \cos(\phi_1)}{N_1 \cos(\phi_0) + N_0 \cos(\phi_1)} = \frac{N_1 \cos(\phi_0) - N_0 \sqrt{1 - \left(\frac{N_0 \sin(\phi_0)}{N_1}\right)^2}}{N_1 \cos(\phi_0) + N_0 \sqrt{1 - \left(\frac{N_0 \sin(\phi_0)}{N_1}\right)^2}} \quad (2)$$

$$r_s = \frac{N_0 \cos(\phi_0) - N_1 \cos(\phi_1)}{N_0 \cos(\phi_0) + N_1 \cos(\phi_1)} = \frac{N_0 \cos(\phi_0) - N_1 \sqrt{1 - \left(\frac{N_0 \sin(\phi_0)}{N_1}\right)^2}}{N_0 \cos(\phi_0) + N_1 \sqrt{1 - \left(\frac{N_0 \sin(\phi_0)}{N_1}\right)^2}} \quad (3)$$

In the Eq (2) and Eq. (3), N_0 is the refractive index of the surrounding medium, $N_1 = n + jk$ is the complex refractive index of the sample. ϕ_0 is the incident angle and ϕ_1 the angle of refraction. These two angles are linked by Snell-Descartes relation. In practice the measurement of ρ (Eq. (1)) gives the value of ψ and Δ , from which one can derived the real part, n , and the imaginary part of the refractive index, k .

Uncertainties on the incident angle and on the phase induced by the windows of the cryostat may induced errors in the evaluation on the refractive index. In the following, errors propagation calculations are done in order to estimate the influence of these parameters on the determination of n and k .

Taking the differential of ρ , one can write

$$d\rho = \frac{\partial \rho}{\partial N_0} dN_0 + \frac{\partial \rho}{\partial N_1} dN_1 + \frac{\partial \rho}{\partial \phi} d\phi \quad (4)$$

Since the surrounding medium is vacuum in our measurements, we can neglect the variation of N_0 . If we rewrite Eq. (4) by ordenning the different terms, one can write :

$$dN_1 = \frac{d\rho - \frac{\partial \rho}{\partial \phi} d\phi}{\frac{\partial \rho}{\partial N_1}} \quad (5)$$

ρ is also defined by the Eq. (1). One can the write $d\rho$ as expressed in Eq. (6). which can be easily differentiated (see Eq. (7)).

$$d\rho = \frac{\partial \rho}{\partial \psi} d\psi + \frac{\partial \rho}{\partial \Delta} d\Delta \quad (6)$$

$$d\rho = \frac{e^{i\Delta}}{\cos^2(\psi)} d\psi + i\rho d\Delta \quad (7)$$

By replacing the expression of $d\rho$ in Eq. (5) by its expression given by Eq. (7), one can write the following expression for dN_1 (see Eq. (8)).

$$dN_1 = \frac{\frac{e^{i\Delta}}{\cos^2(\psi)} d\psi + i\rho d\Delta - \frac{\partial \rho}{\partial \phi} d\phi}{\frac{\partial \rho}{\partial N_1}} \quad (8)$$

From the expression of the reflection coefficient, r_s and r_p , and from the definition of ρ , one can derived the expressions of $\frac{\partial \rho}{\partial \phi}$ (Eq. 9) and $\frac{\partial \rho}{\partial N_1}$ (Eq. 10).

$$\frac{\partial \rho}{\partial \phi} = - \frac{\frac{\partial \rho}{\partial N_1} \left(N_1^2 \left(1 + \frac{1}{\cos^2(\phi)} \right) + N_0^2 \left(1 - \frac{1}{\cos^2(\phi)} \right) \right)}{N_1 \tan(\phi)} \quad (9)$$

$$\frac{\partial \rho}{\partial N_1} = - \frac{N_1 (1 + \rho)^3 \cos^2(\phi)}{2(1 - \rho) N_0 \sin^4(\phi)} \quad (10)$$

Each term in the Eq. (8) are known. If one writes the sample refractive index as $N_1 = n + jk$, then error propagation can be written as Eq. (1),

$$dN_1 = a_1 d\phi + a_2 d\Delta + a_3 d\psi \quad (8)$$

where $d\phi$ is the uncertainty on the incidence angle, $d\Delta$ is the error made in the estimation of the phase shift and $d\psi$ is the uncertainty related to wave amplitude calculations. a_1 , a_2 and a_3 are defined by equations Eq. (9), Eq. (10) and Eq. (11).

$$a_1 = \frac{N_1^2 \left(1 + \frac{1}{\cos^2(\phi)}\right) + N_0^2 \left(1 - \frac{1}{\cos^2(\phi)}\right)}{N_1 \tan(\phi)} \quad (9)$$

$$a_2 = \frac{2i\rho(\rho - 1)}{N_1(1 + \rho^3)} n_0^2 \sin^2(\phi) \tan^2(\phi) \quad (10)$$

$$a_3 = \frac{2(\rho - 1)}{N_1(1 + \rho)^3} N_0^2 \tan^4(\phi) e^{i\Delta} \quad (11)$$

Eventually, errors in the value of n and k are derived by taking the real part and the imaginary part of dN_1 respectively.

References

- [1] S. del Sordo, L. Abbene, E. Caroli, A. M. Mancini, A. Zappettini, et P. Ubertini, « Progress in the development of CdTe and CdZnTe semiconductor radiation detectors for astrophysical and medical applications », *Sensors*, vol. 9, n° 5, p. 3491-3526, 2009, doi: 10.3390/s90503491.
- [2] C. Ferekides et J. Britt, « CdTe solar cells with efficiencies over 15% », *Solar Energy Materials and Solar Cells*, 1994, doi: 10.1016/0927-0248(94)90148-1.
- [3] A. Rogalski, « Infrared detectors: Status and trends », *Progress in Quantum Electronics*, vol. 27, n° 2-3, p. 59-210, 2003, doi: 10.1016/S0079-6727(02)00024-1.
- [4] S. D. Johnson *et al.*, « Radiation effects in WFC3 IR detectors », *Focal Plane Arrays for Space Telescopes*, vol. 5167, p. 243, 2004, doi: 10.1117/12.508443.
- [5] A. Waczynski *et al.*, « Radiation induced luminescence of the CdZnTe substrate in HgCdTe detectors for WFC3 », 2006. doi: 10.1117/12.617716.
- [6] R. Smith *et al.*, « Noise and zero point drift in 1.7 μ m cutoff detectors for SNAP », *High Energy, Optical, and Infrared Detectors for Astronomy II*, vol. 6276, p. 62760R, 2006, doi: 10.1016/j.coastaleng.2011.06.009.
- [7] A. Waczynski *et al.*, « Radiation induced luminescence of the CdZnTe substrate in HgCdTe detectors for WFC3 », in *Focal Plane Arrays for Space Telescopes II*, San Diego, California, USA, août 2005, p. 59020P. doi: 10.1117/12.617716.
- [8] R. Smith *et al.*, « Noise and zero point drift in 1.7 μ m cutoff detectors for SNAP », in *High Energy, Optical, and Infrared Detectors for Astronomy II*, juin 2006, vol. 6276, p. 62760R. doi: 10.1117/12.672616.
- [9] M. L. Dorn *et al.*, « Proton irradiation results for long-wave HgCdTe infrared detector arrays for Near-Earth Object Camera », *JATIS*, vol. 2, n° 3, p. 036002, août 2016, doi: 10.1117/1.JATIS.2.3.036002.
- [10] M. L. Dorn *et al.*, « Proton irradiation results for long-wave HgCdTe infrared detector arrays for Near-Earth Object Camera », *Journal of Astronomical Telescopes, Instruments, and Systems*, vol. 2, n° 3, p. 036002, 2016, doi: 10.1117/1.JATIS.2.3.036002.
- [11] T. Pichon, S. Mouzali, O. Boulade, O. Gravrand, et O. Limousin, « Influence of the CdZnTe Substrate Thickness on the Response of HgCdTe Detectors Under Irradiation: Modeling of the Substrate Luminescence », *Journal of Elec Materi*, juin 2020, doi: 10.1007/s11664-020-08237-0.
- [12] T. L. Goff *et al.*, « ROIC glow reduction in very low flux short wave infra-red focal plane arrays for astronomy. », Paris, 2020, p. 6.
- [13] T. Pichon *et al.*, « Experimental study of the influence of the CdZnTe substrate thickness on the response of infrared HgCdTe photodetectors under proton irradiation », in *X-Ray, Optical, and Infrared Detectors for Astronomy IX*, déc. 2020, vol. 11454, p. 114540O. doi: 10.1117/12.2562142.
- [14] D. J. Olego, J. P. Faurie, S. Sivananthan, et P. M. Raccach, « Optoelectronic properties of Cd_{1-x}Zn_xTe films grown by molecular beam epitaxy on GaAs substrates properties of Cd_{1-x}Zn_xTe films grown by molecular beam epitaxy on GaAs substrates », vol. 1172, p. 1-4, 1985, doi: 10.1063/1.96316.
- [15] F. Molva, J. P. Chamonal, et J. L. Pautrat, « Shallow Acceptors in Cadmium Telluride », *physica status solidi (b)*, vol. 109, n° 2, p. 635-644, févr. 1982, doi: 10.1002/pssb.2221090222.
- [16] H. Y. Shin et C. Y. Sun, « The exciton and edge emissions in CdTe crystals », *Materials Science and Engineering B*, vol. 52, n° 1, p. 78-83, 1998, doi: 10.1016/S0921-5107(97)00145-1.

- [17] G. Fonthal, L. Tirado-Mejía, J. I. Marín-Hurtado, H. Ariza-Calderón, et J. G. Mendoza-Alvarez, « Temperature dependence of the band gap energy of crystalline CdTe », *Journal of Physics and Chemistry of Solids*, 2000, doi: 10.1016/S0022-3697(99)00254-1.
- [18] S. Jain, « Photoluminescence study of cadmium zinc telluride », *Ph.D dissertation, West Virginia University*, 2001.
- [19] J. M. Francou, K. Saminadayar, et J. L. Pautrat, « Shallow donors in CdTe », *Physical Review B*, 1990, doi: 10.1103/PhysRevB.41.12035.
- [20] J. Lee et N. C. Giles, « Low-temperature photoluminescence from bulk CdTe and Cd_{0.967}Zn_{0.033}Te », *Journal of Applied Physics*, 1995, doi: 10.1063/1.360356.
- [21] J. P. Chamonal, E. Molva, et J. L. Pautrat, « Identification of Cu and Ag acceptors in CdTe », *Solid State Communications*, 1982, doi: 10.1016/0038-1098(82)90843-2.
- [22] K. Hjelt, M. Juvonen, T. Tuomi, S. Nenonen, E. E. Eissler, et M. Bavdaz, « Photoluminescence of Cd_{1-x}Zn_xTe crystals grown by high-pressure bridgman technique », *Physica Status Solidi (A) Applied Research*, vol. 162, n° 2, p. 747-763, 1997, doi: 10.1002/1521-396X(199708)162:2<747::AID-PSSA747>3.0.CO;2-2.
- [23] J. Lee, N. C. Giles, D. Rajavel, et C. J. Summers, « Room-temperature band-edge photoluminescence from cadmium telluride », *Physical Review B*, vol. 49, n° 3, p. 1668-1676, janv. 1994, doi: 10.1103/PhysRevB.49.1668.
- [24] P. Capper, *Properties of narrow gap cadmium-based compounds*. London, 1995. doi: 10.1016/0961-1290(95)80115-4.
- [25] P. Horodyský et P. Hlídaek, « Free-exciton absorption in bulk CdTe: Temperature dependence », *Physica Status Solidi (B) Basic Research*, vol. 243, n° 2, p. 494-501, 2006, doi: 10.1002/pssb.200541402.
- [26] F. Gemain, « Etudes spectroscopiques du dopage dans les matériaux II-VI pour les détecteurs infrarouge et les cellules photovoltaïques », Université Joseph Fourier - Grenoble I, 2012.
- [27] S. P. Tobin *et al.*, « A comparison of techniques for nondestructive composition measurements in CdZnTe substrates », *Journal of Electronic Materials*, vol. 24, n° 5, p. 697-705, 1995, doi: 10.1007/BF02657981.
- [28] J. L. Reno et E. D. Jones, « Determination of the dependence of the band-gap energy on composition for Cd_{1-x}Zn_xTe », *Physical Review B*, vol. 45, n° 3, p. 1440-1442, 1992, doi: 10.1103/PhysRevB.45.1440.
- [29] K. Oettinger, D. M. Hofmann, Al. L. Efros, B. K. Meyer, M. Salk, et K. W. Benz, « Excitonic line broadening in bulk grown Cd_{1-x}Zn_xTe », *Journal of Applied Physics*, vol. 71, n° 9, p. 4523-4526, 2002, doi: 10.1063/1.350798.
- [30] P. Y. Yu et M. Cardona, *Fundamentals of Semiconductors*. Berlin, Heidelberg: Springer Berlin Heidelberg, 2010. doi: 10.1007/978-3-642-00710-1.
- [31] E. Molva, J. L. Pautrat, K. Saminadayar, G. Milchberg, et N. Magnea, « Acceptor states in CdTe and comparison with ZnTe. General trends », *Physical Review B*, 1984, doi: 10.1103/PhysRevB.30.3344.
- [32] C. B. Norris et C. E. Barnes, « Cathodoluminescence studies of the 1.4 eV bands in CdTe », *Revue de Physique Appliquée*, 1977, doi: 10.1051/rphysap:01977001202021900.
- [33] M. Fiederle, A. Fauler, J. Konrath, V. Babentsov, J. Franc, et R. B. James, « Comparison of undoped and doped high resistivity CdTe and (Cd,Zn)Te detector crystals », 2004. doi: 10.1109/TNS.2004.832958.
- [34] J. Krustok, V. Valdna, K. Hjelt, et H. Collan, « Deep center luminescence in p-type CdTe », *Journal of Applied Physics*, 1996, doi: 10.1063/1.362981.
- [35] K. Lischka, G. Brunthaler, et W. Jantsch, « Deep donor levels due to isolated Fe in CdTe », *Journal of Crystal Growth*, vol. 72, p. 355-259, 1985.
- [36] D. Kuciauskas, A. Kanevce, P. Dippo, S. Seyedmohammadi, et R. Malik, « Minority-carrier lifetime and surface recombination velocity in single-crystal CdTe », *IEEE Journal of Photovoltaics*, vol. 5, n° 1, p. 366-371, 2015, doi: 10.1109/JPHOTOV.2014.2359738.
- [37] R. Triboulet et P. Siffert, *CdTe and Related Compounds; Physics, Defects, Hetero- and Nano-structures, Crystal Growth, Surfaces and Applications*. Elsevier, 2010. doi: 10.1016/C2009-0-61369-6.
- [38] S. Hildebrandt, H. Uniewski, J. Schreiber, et H. S. Leipner, « Localization of Y luminescence at glide dislocations in cadmium telluride », *Journal de Physique III*, 1997, doi: 10.1051/jp3:1997203.
- [39] A. Castaldini, A. Cavallini, B. Fraboni, et L. Polenta, « Cathodoluminescence and photoinduced current spectroscopy studies of defects in Cd_{0.8}Zn_{0.2}Te », vol. 54, n° 11, p. 7622-7625, 1996.
- [40] Z. F. Li, W. Lu, G. S. Huang, J. R. Yang, L. He, et S. C. Shen, « Microphotoluminescence mapping on CdZnTe: Zn distribution », *Journal of Applied Physics*, vol. 90, n° 1, p. 260, 2001, doi: 10.1063/1.1378062.
- [41] S. John, C. Soukoulis, M. H. Cohen, et E. N. Economou, « Theory of Electron Band Tails and the Urbach Optical-Absorption Edge », *Phys. Rev. Lett.*, vol. 57, n° 14, p. 1777-1780, oct. 1986, doi: 10.1103/PhysRevLett.57.1777.
- [42] N. Bouarissa, « Pseudopotential calculations of Cd_{1-x}Zn_xTe : Energy gaps and dielectric constants », vol. 399, p. 126-131, 2007, doi: 10.1016/j.physb.2007.05.034.
- [43] M. Prokesch et C. Szeles, « Accurate measurement of electrical bulk resistivity and surface leakage of CdZnTe radiation detector crystals », *Journal of Applied Physics*, 2006, doi: 10.1063/1.2209192.

- [44] F. G. Sanchez-Almazan *et al.*, « Temperature dependence of the band gap of Cd_{1-x}Zn_xTe alloys of low zinc concentrations », *Journal of Applied Physics*, vol. 79, p. 7713, 1996.
- [45] R. Pässler, « Temperature dependence of fundamental band gaps in group IV, III-V, and II-VI materials via a two-oscillator model », *Journal of Applied Physics*, 2001, doi: 10.1063/1.1369407.
- [46] J. P. Laurenti, J. Camassel, A. Bouhemadou, B. Toulouse, R. Legros, et A. Lusson, « Temperature dependence of the fundamental absorption edge of mercury cadmium telluride », *Journal of Applied Physics*, 1990, doi: 10.1063/1.345119.
- [47] Jeong, T. S. et Yu, P. Y., « Temperature Dependence of the Photocurrent in p-Type CdTe », *J. Korean, Phys. Soc.*, 2003.
- [48] D. Chandler-Horowitz, *Semiconductor measurement technology: analytic analysis of ellipsometric errors*. National Bureau of Standards Special Publication, 1986.
- [49] J. D. Jackson, *Classical electrodynamics*, 3rd ed. New York: Wiley, 1999.
- [50] S. Adachi *et al.*, « Related content Optical Constants of Zn_{1-x}Cd_xTe Ternary Alloys : Experiment and Modeling », *Japanese Journal of Applied Physics*, vol. 32, n° 8R, p. 3496, 1993.
- [51] D. T. F. Marple, « Optical absorption edge in CdTe: Experimental », *Physical Review*, vol. 150, n° 2, p. 728-734, 1966, doi: 10.1103/PhysRev.150.728.
- [52] P. Hlídek, J. Bok, J. Franc, et R. Grill, « Refractive index of CdTe: Spectral and temperature dependence », *Journal of Applied Physics*, 2001, doi: 10.1063/1.1385351.
- [53] E. Finkman, S. E. Schacham, E. Finkman, et S. E. Schacham, « The exponential optical absorption band tail of Hg_{1-x}Cd_xTe The exponential J », vol. 2896, n° 1984, 1994, doi: 10.1063/1.333828.
- [54] P. Hlídek, J. Bok, J. Franc, et R. Grill, « Refractive index of CdTe: Spectral and temperature dependence », *Journal of Applied Physics*, vol. 90, n° 3, p. 1672-1674, août 2001, doi: 10.1063/1.1385351.
- [55] T. Materials, M. A. Quijada, et R. Henry, « Temperature Evolution of Excitonic Absorptions in Cd-, Zn, Te Materials », *Proc. SPIE 6692, Cryogenic Optical Systems and Instruments XII*, 2007, doi: 10.1117/12.735604.
- [56] J. Hamann *et al.*, « Identification of Ag-acceptor related photoluminescence in 111Ag doped CdTe », *Applied Physics Letters*, 1998, doi: 10.1063/1.121530.
- [57] P. Capper, *Properties of Narrow Gap Cadmium-based Compounds*. IET, 1994.
- [58] S. Seto, A. Tanaka, Y. Masa, S. Dairaku, et M. Kawashima, « Annealing behavior of bound exciton lines in high quality CdTe », *Appl. Phys. Lett.*, vol. 53, n° 16, p. 1524-1526, oct. 1988, doi: 10.1063/1.99945.